4

Theoretical Foundations of Noise Interferometry

ANDREAS FICHTNER AND VICTOR C. TSAI

Abstract

The retrieval of a deterministic signal from recordings of a quasi-random ambient seismic field is the central goal of noise interferometry. It is the foundation of numerous applications ranging from noise source imaging to seismic tomography and time-lapse monitoring. In this chapter, we offer a presentation of theoretical approaches to noise interferometry, complemented by a critical discussion of their respective advantages and drawbacks.

The focus of this chapter is on interstation noise correlations that approximate the Green's function between two receivers. We explain in detail the most common mathematical models for Green's function retrieval by correlation, including normal-mode summation, plane-wave decomposition, and representation theorems. While the simplicity of this concept is largely responsible for its remarkable success, each of these approaches rests on different but related assumptions such as wavefield equipartitioning or a homogeneous distribution of noise sources. Failure to meet these conditions on Earth may lead to biases in traveltimes, amplitudes, or waveforms in general, thereby limiting the accuracy of the method.

In contrast to this well-established method, interferometry without Green's functional retrieval does not suffer from restrictive conditions on wavefield equipartitioning. The basic concept is to model the interstation correlation directly for a given power-spectral density distribution of noise sources and for a suitable model of the Earth that may be attenuating, heterogeneous, and anisotropic. This approach leads to a coupled problem where both structure and sources affect data, much like in earthquake tomography. Observable variations of the correlation function are linked to variations in Earth structure and noise sources via finite-frequency sensitivity kernels that can be used to solve inverse problems. While being mathematically and computationally more complex, interferometry without Green's function retrieval has produced promising initial results that make successful future applications likely.

We conclude this chapter with a summary of alternative approaches to noise interferometry, including interferometry by deconvolution, multi-dimensional deconvolution, and iterated correlation of coda waves.

4.1 Introduction

Noise is unwanted, unpleasant, or loud sound, according to the *Cambridge English Dictionary*. This unflattering description carries a historical connotation of uselessness that hardly reflects the wide range of present-day applications that exploit the omnipresent noise field of the Earth. Seismic noise on Earth is not random *sensu stricto*. Its propagation is governed by the laws of physics that imprint structure on the wavefield. This structure can be exploited using interferometry that "turns noise into signal" (Curtis et al., 2006).

While the pioneering work of Aki (1957) suggested early on that statistical properties of seismic noise may be used to infer Earth structure, practical efforts to extract interpretable information were often found to be more challenging than suggested by seemingly simple theories (e.g., Claerbout, 1968; Cole, 1995). Although seismic interferometry requires only two seismic stations, or a single station for autocorrelations, the ambient wavefield only became widely used in seismic tomography when large, dense arrays started to offer unprecedented illumination of the Earth's crust (e.g., Sabra et al., 2005; Shapiro et al., 2005).

Today, the large majority of ambient noise tomography results are ostensibly based on Green's function retrieval, that is, the assumption that the Green's function between two stations is approximated by the time-averaged cross-correlation of noise. By treating correlation-based Green's function approximations as conventional earthquake or active-source signals, already established tomographic methods can be used to estimate subsurface properties. Green's function retrieval can be observed in laboratory experiments (e.g., Malcolm et al., 2004; van Wijk, 2006; Nooghabi et al., 2017), and it can be justified theoretically using normal-mode, plane-wave, representation-theorem, or purely numerical approaches (e.g., Lobkis and Weaver, 2001; Snieder, 2004a; Wapenaar and Fokkema, 2006; Cupillard, 2008; Tsai, 2009; Cupillard and Capdeville, 2010; Boschi et al., 2013).

During the past decade, interferometry based on interstation correlations of ambient noise has become a standard tool. In seismic exploration, interferometry is an inexpensive alternative to active-source imaging and monitoring (e.g., Bussat and Kugler, 2011; Mordret et al., 2013, 2014; de Ridder et al., 2014; de Ridder and Biondi, 2015; Nakata et al., 2015; Delaney et al., 2017). Improved coverage in regions that are less well illuminated by earthquakes has advanced regional crustal studies (e.g., Sabra et al., 2005; Shapiro et al., 2005; Stehly et al., 2009; Shapiro, 2018), continental- and global-scale tomography (e.g., Lin et al.,

2008; Zheng et al., 2011; Verbeke et al., 2012; Saygin and Kennett, 2012; Nishida and Montagner, 2009; Kao et al., 2013; Haned et al., 2016), and the imaging of deep internal discontinuities (e.g., Poli et al., 2012; Boué et al., 2013; Poli et al., 2015) and the inner core (e.g., Lin et al., 2013; Huang et al., 2016). Furthermore, the omnipresence of ambient noise has enabled the long-term investigation of time-dependent subsurface structures along active fault zones, beneath volcanoes, and within geothermal reservoirs (e.g., Brenguier et al., 2008a,b; Obermann et al., 2013, 2014, 2015; Hillers et al., 2015; Sens-Schönfelder and Brenguier, 2018; Snieder et al., 2018).

In general, theories for Green's function retrieval rely on the assumption that the ambient wavefield is equipartitioned, meaning that all propagation modes are equally strong and statistically uncorrelated. Equipartitioning may arise either directly through the action of uncorrelated and homogeneously distributed noise sources, or indirectly through sufficiently strong multiple scattering.

In the Earth, wavefields are not generally equipartitioned for various reasons. Scattering may be too weak and attenuation too strong to produce significant multiple scattering; and the distribution of noise sources is strongly heterogeneous, and time-variable (see Chapters 1–3 [McNamara et al., 2018; Gal and Reading, 2018; Ardhuin et al., 2018]). While the frequency-dependent arrival times of fundamental-mode surface waves are empirically found to be rather robust, other components of the wavefield suffer from not meeting the requirements for Green's function retrieval. Well-documented problems include travel time and amplitude errors, incorrect higher-mode surface waves, the presence of spurious arrivals, and the weakness or complete absence of body waves (e.g., Halliday and Curtis, 2008; Tsai, 2009; Kimman and Trampert, 2010; Froment et al., 2010; Forghani and Snieder, 2010; Fichtner, 2014; Kästle et al., 2016). This has, so far, prevented the application of finite-frequency and full-waveform inversion techniques that exploit complete waveforms for the benefit of improved resolution (e.g., Igel et al., 1996; Pratt, 1999; Friederich, 2003; Yoshizawa and Kennett, 2004; Zhou et al., 2006; Fichtner et al., 2009; Tape et al., 2010).

Concepts to circumvent these drawbacks and to establish a variant of interferometry without Green's function retrieval originated in helioseismology, though wavefields in the Sun are far more equipartitioned than in the Earth (Woodard, 1997; Gizon and Birch, 2002; Hanasoge et al., 2011). Interferometry without Green's function retrieval makes no assumptions on the distribution of noise sources or the properties of the wavefield. Instead, interstation correlations can be computed for any distribution of noise sources and any type of medium. Information on both the noise sources and structure of the Earth may then be extracted through the comparison with observed correlations and the computation

of sensitivity kernels (e.g., Tromp et al., 2010; Hanasoge, 2013; Hanasoge and Branicki, 2013; Fichtner et al., 2017a; Sager et al., 2018).

In the following sections, we summarize the most prevalent theories for Green's function retrieval by correlation, which are based on normal-mode summation, plane-wave decomposition, and representation theorems, respectively. Subsequently, we outline the basic concepts of interferometry without Green's function retrieval. Finally, we discuss alternative approaches to seismic interferometry, as well as possible future directions of research.

4.2 Normal-Mode Summation

Perhaps the simplest context in which a theoretical result exists linking correlations of noise recorded at two points to the Green's function between those points is for acoustic normal modes in a finite body. It is this case that we shall consider first, and for which we will give a fairly complete derivation. For this case, the equation governing motion is the acoustic wave equation,

$$\frac{1}{\kappa(\mathbf{x})}\frac{\partial^2}{\partial t^2}u(\mathbf{x},t) - \frac{\partial}{\partial x_i}\left(\frac{1}{\rho(\mathbf{x})}\frac{\partial}{\partial x_i}u(\mathbf{x},t)\right) = f(\mathbf{x},t), \tag{4.1}$$

where $\mathbf{x}$ is the position vector, κ is bulk modulus, ρ density, and f the external forcing that excites the pressure wavefield u. Throughout this chapter we employ the summation convention, meaning that summation of repeated indices is implicit. The various normal modes that solve equation (4.1) with vanishing right-hand side can be expressed generally as

$$u_p(\mathbf{x},t) = s_p(\mathbf{x})\cos(\omega_p t + \phi_p), \tag{4.2}$$

where $s_p(\mathbf{x})$ is the spatial mode shape or eigenfunction, ω_p is the frequency of the mode, and ϕ_p is the phase of the mode. For the derivation provided below, it is not necessary to know the precise shape of each mode. The only property used will be that the modes are orthogonal in both space and time. For spatial orthogonality, this implies that $\int s_m(\mathbf{x})s_n(\mathbf{x})d\mathbf{x} = 0$ if $m \neq n$; for temporal orthogonality, this implies that $\int \cos(\omega_m t + \phi_m)\cos(\omega_n t + \phi_n)dt = 0$ if $\omega_m \neq \omega_n$. It should be noted that in realistic media, many modes can share the same or close to the same frequency, leading to a more complex result as will be discussed below (Tsai, 2010). As a simple example that may help with intuition, one may consider the homogeneous one-dimensional string with fixed end points at $x = 0$ and $x = L$, for which the spatial modes can be explicitly written as $\sin(n\pi x/L)$ with corresponding frequency $\omega_n = n\pi c/L$, with c being the homogeneous wave speed. Spatial orthogonality reduces to the result that $\int \sin(m\pi x/L)\sin(n\pi x/L)dx = 0$ for $m \neq n$ (e.g., Haberman, 2013).

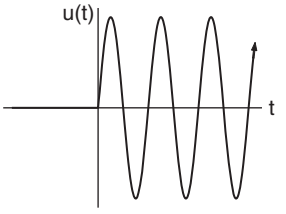

Figure 4.1. Schematic illustration of the Green's function from equation (4.3).

Part of the reason that a normal-mode framework is particularly straightforward is that (1) Green's functions are particularly easy to describe, and (2) the noise correlation simplifies due to the orthogonality property. For each mode, the spatial orthogonality relation can be used to show that the Green's function is described by (e.g., Snieder, 2004b)

$$G_p(\mathbf{x}, \mathbf{x}_s, t) = \begin{cases} \frac{s_p(\mathbf{x}) s_p(\mathbf{x}_s)}{\omega_p} \sin(\omega_p t), & \text{for } t > 0, \\ 0, & \text{for } t < 0, \end{cases} \tag{4.3}$$

which is schematically shown in Figure 4.1. In other words, each mode oscillates as a sinusoid starting at $t = 0$, and the full Green's function is a sum over these components, $G = \sum_{p=0}^{\infty} G_p$ (e.g., Gilbert, 1970; Haberman, 2013).

Defining the normalized cross-correlation of two arbitrary functions f and g as

$$C[f(t), g(t)] = \lim_{T \to \infty} \frac{1}{2T} \int_{-T}^{T} f(\tau) g(\tau + t) d\tau, \tag{4.4}$$

then for an arbitrary general wavefield $u(\mathbf{x}, t) = \sum_p A_p u_p(\mathbf{x}, t)$, the temporal orthogonality property immediately results in many cross terms disappearing in the cross-correlation. Specifically, if all ω_p are different (see below for the more general case) then direct calculation shows that the cross-correlation of recordings at positions $\mathbf{x}_A$ and $\mathbf{x}_B$ reduces to

$$C(\mathbf{x}_A, \mathbf{x}_B) = C[u(\mathbf{x}_A, t), u(\mathbf{x}_B, t)] = \frac{1}{2} \sum_{p=0}^{\infty} A_p^2 s_p(\mathbf{x}_A) s_p(\mathbf{x}_B) \cos(\omega_p t). \tag{4.5}$$

Comparing equations (4.3) and (4.5), it is thus clear that there is a potential relationship between the Green's function and the cross-correlation. The most commonly quoted version of this is that if $A_p = \alpha/\omega_p$, with α an arbitrary constant, then

$$\frac{d}{dt} C(\mathbf{x}_A, \mathbf{x}_B) = -\frac{\alpha^2}{2} [G(\mathbf{x}_A, \mathbf{x}_B, t) - G(\mathbf{x}_A, \mathbf{x}_B, -t)]. \tag{4.6}$$

This statement says that if energy happens to be equipartitioned between all of the modes and hence amplitudes are weighted inversely with frequency, then the

time derivative of the cross-correlation between two stations is equal to the sum of a Green's function and a time-reversed Green's function between those same two points, up to a normalization factor. Alternatively, if modal amplitudes are all equal such that $A_p = \alpha$, then

$$C(\mathbf{x}_A, \mathbf{x}_B) = \frac{\alpha^2}{2} \frac{d}{dt} [G(\mathbf{x}_A, \mathbf{x}_B, t) - G(\mathbf{x}_A, \mathbf{x}_B, -t)]. \tag{4.7}$$

In other words, if modal amplitudes are all equal, then the cross-correlation between two stations is equal to the time derivative of the sum of a Green's function and its time-reversed version between those same two points, again up to a normalization factor.

The two relationships (4.6) and (4.7) appear different, but in fact express the same identity. Since a time derivative results in a phase advance of 90°, it is clear that both identities express the fact that each modal component of the cross-correlation is expected to be phase advanced by 90° with respect to each modal component of the Green's function. This is also clear simply by comparing the sine term of equation (4.3) with the cosine term of equation (4.5).

It is important to note two related points. Firstly, so far, the identities hold for a deterministic process, and do not require any "noise" property to hold. Secondly, however, as mentioned above, the identities require all modes to have different frequencies. This is clearly not expected in general. For example, on the Earth, two waves arriving from two different azimuths can easily have frequency content that is similar. Resolution to this issue occurs if cross-terms from modes with the same frequency still somehow cancel out, despite not satisfying the temporal orthogonality property. For "noise" sources, this may occur if the sources are uncorrelated over long timescales. For example, take the case above of two waves created by two different wave sources, which could be two different ocean storms, at two different azimuths. If the two sources randomly change their relative phase over time, rather than staying correlated over all time as a deterministic signal would, and if there is at least a small amount of damping in the system such that waves excited at one instance in time do not keep contributing forever, then eventually the cross-correlation between these two different sources would be expected to cancel out and sum to zero. This cancellation of different uncorrelated noise sources has been discussed by many authors (e.g., Lobkis and Weaver, 2001; Tsai, 2010), most of whom treat each independent time period as a separate "realization" of an ensemble, and these authors have shown that the cancellation of noise occurs proportionally to the square root of time. While the above argument is a heuristic one, a mathematically rigorous derivation is possible that demonstrates that spatially uncorrelated sources can result in uncorrelated modes (e.g., Lobkis and Weaver,

2001), but this is beyond the scope of this work. The final result is an identity similar to equation (4.6) that states

$$\frac{d}{dt}C[u^N(\mathbf{x}_A, t), u^N(\mathbf{x}_B, t)] = -\frac{\alpha^2}{2}[G(\mathbf{x}_A, \mathbf{x}_B, t) - G(\mathbf{x}_A, \mathbf{x}_B, -t)], \qquad (4.8)$$

if $A_p = \alpha/\omega_p$ and u^N is a "noise" field for which each mode still vibrates sinusoidally in time, but is temporally uncorrelated with all other modes over long enough times, with the properties discussed in the previous paragraph. This is perhaps the most commonly quoted Green's function-noise correlation identity.

So far, only the simplest case of acoustic waves has been considered. However, all of the arguments made above also work for modes of the elastic wave equation with only minor modifications. For example, for vertical-component Rayleigh modes, one can still write a mode sum in the same manner, and equation (4.8) still holds in the same way.

The primary issue with the normal mode derivation is that the assumptions are extremely limiting. For example, modes on Earth are certainly never close to equipartitioned for at least two reasons. For one, the majority of noise sources on Earth are expected to be at or near the Earth's surface (e.g., ocean waves, wind, industrial activity, traffic) and such surface sources excite fundamental-mode waves much more strongly than they excite higher-order modes. Thus, these different types of modes will have vastly different amounts of energy (and will have very different modal amplitudes), implying that the conditions for the identities to hold are not satisfied. Moreover, even within the subset of fundamental-mode waves, the fact that large noise sources, like ocean storms, are concentrated spatially in certain areas of the Earth implies that waves from certain directions will be much stronger and will therefore not be close to equipartitioned. Since the assumptions resulting in equation (4.8) are not valid on the Earth, the result is not expected to be generally exact. Moreover, within the normal-mode framework, it is not clear how to evaluate how closely to achieving (4.8) noise correlations are likely to be for a realistic distribution of seismic noise on Earth.

4.3 Plane Waves

Given that the assumptions of the normal-mode derivation are not expected to hold on the Earth, it is worthwhile to consider other reasons why the identity of equation (4.8) still might hold or at least approximately hold. Our path forward is to consider the case of plane surface waves incident on a pair of stations, $\mathbf{x}_A$ and $\mathbf{x}_B$, as before. One may note that for waves with wavelengths that are a small fraction of the radius of a weakly heterogeneous Earth, there is an equivalence between plane waves and normal modes. Plane waves are simply the propagating mode produced

by a far-field source that corresponds to the standing wave of the normal-mode framework. For a homogeneous halfspace, it may be useful to note that the equipartition assumption would imply an equal amplitude of energy incoming from all azimuths (e.g., Weaver and Lobkis, 2004). Due to this equivalence, it would be natural to assume that a similar Green's function cross-correlation identity should exist specifically for this case in which "noise" energy is equally incident from all directions. While using only far-field sources means that near-field sources are excluded from this description, one may argue that as long as the body (like the Earth) is large enough and attenuation is relatively small, the far-field contribution might be expected to dominate the energy from near-field sources, thus leading to the expectation that an identity might exist even when using far-field sources only.

To derive this identity, one can again simply write down the Green's function for surface waves in a homogeneous, acoustic, non-attenuating medium and compare it to the correlation of far-field plane-wave sources. The Green's function for waves in a homogeneous 2D medium can be expressed in the frequency domain as

$$G(\mathbf{x}, \mathbf{x}_s, \omega) = \frac{-i}{4}\mathcal{H}_0^{(2)}(kr), \tag{4.9}$$

where $\mathcal{H}_0^{(2)}$ is a Hankel function of order zero of the second kind, $k = \omega/c$ is wavenumber, $\mathbf{x}_s$ is the source position, and $r = |\mathbf{x} - \mathbf{x}_s|$. (See, e.g., Morse and Feshbach (1953) or Snieder (2004b) for derivations of equation (4.9) though these use slightly different Fourier conventions than assumed here.) Again, we write only the result for the 2D acoustic case, but anticipate the elastic case having the same form, for instance, for Rayleigh waves in a laterally homogeneous 3D medium. The far-field, time-domain version of this expression (e.g., Watson, 2008) is perhaps more easily recognized:

$$G(\mathbf{x}, \mathbf{x}_s, t) = \sqrt{\frac{1}{8\pi kr}}\cos[\omega t - (kr + \pi/4)]. \tag{4.10}$$

On the other hand, a general sum of far-field plane waves can be expressed as

$$u(\mathbf{x}, t) = \frac{1}{2\pi}\int_0^{2\pi} A(\theta)\cos(\omega t - kr)\, d\theta \tag{4.11}$$

where the plane-wave density of sources at each azimuth is given by $A(\theta)$, and r is the distance from the far-field source to $\mathbf{x}$. Just as in the normal-mode case, if we again assume that the plane wave sources from different azimuths are all uncorrelated, then eventually all cross-terms in the cross-correlation will cancel out and sum to zero, leaving only

$$C[u(\mathbf{x}_A, t), u(\mathbf{x}_B, t)] = \frac{1}{8\pi^2}\int_0^{2\pi} A(\theta)^2\cos(\omega t - k\Delta x\cos\theta)\, d\theta, \tag{4.12}$$

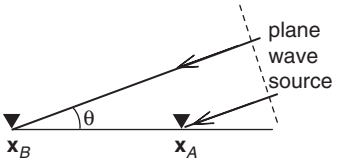

Figure 4.2. Schematic illustration of a plane wave reaching receiver positions $\mathbf{x}_A$ and $\mathbf{x}_B$.

where Δx is the distance between $\mathbf{x}_A$ and $\mathbf{x}_B$, and θ is the azimuth of the source relative to the line between $\mathbf{x}_A$ and $\mathbf{x}_B$ (see Figure 4.2). Note that unlike in the normal-mode case, there is a phase shift for each plane wave that accounts for the time delay between when the wave arrives at $\mathbf{x}_B$ and $\mathbf{x}_A$.

At this point, it is useful to recognize that the integral can be computed exactly if $A(\theta) = \alpha$ is constant, and can be approximated using the stationary-phase approximation even if $A(\theta)$ is not constant with azimuth. Qualitatively, the stationary-phase approximation can be understood as saying that the primary contributions to an oscillatory integral, like equation (4.12), occur from points where the oscillation phase is stationary, and all other contributions approximately cancel out due to there being equal positive and negative contributions from nearby points (e.g., Båth, 1968; Bender and Orszag, 1999). The end result is that the final integral can be approximated by substituting constant values of the non-oscillatory part of the integrand at the stationary points and integrating only over these stationary points. In the case of equation (4.12), there are two stationary-phase points at $\theta = 0°$ and $\theta = 180°$, so that the stationary-phase argument can be used to approximate the original integral as

$$C(\mathbf{x}_A, \mathbf{x}_B, t) \propto \int_{-\pi/2}^{\pi/2} A_+^2 \cos(\omega t - k\Delta x \cos\theta)\, d\theta + \int_{\pi/2}^{3\pi/2} A_-^2 \cos(\omega t - k\Delta x \cos\theta)\, d\theta, \tag{4.13}$$

where $A_+ \equiv A(0°)$, $A_- \equiv A(180°)$, and the two primary contributions come from the two stationary-phase points at azimuths in line with the two stations. Equation (4.13) can then be evaluated by direct integration (without a further stationary-phase approximation to the integral) as

$$C(\mathbf{x}_A, \mathbf{x}_B, t) \propto A_+^2[J_0(k\Delta x)\cos(\omega t) + H_0(k\Delta x)\sin(\omega t)] + A_-^2[J_0(k\Delta x)\cos(\omega t) - H_0(k\Delta x)\sin(\omega t)], \tag{4.14}$$

where J_0 and H_0 are Bessel functions and Struve functions of order zero, respectively (Watson, 2008). Although Struve functions are not a common special function, they are closely related to Bessel functions, and can be thought of as pairing with Bessel functions much like sine and cosine pair together. Since

the stationary-phase approximation is a high-frequency approximation, as long as ω is high enough or $A(\theta)$ is close enough to constant and nonzero at the stationary-phase points, equation (4.14) will be an accurate approximation.

Considering each of the two terms of equation (4.14) separately, and taking a far-field approximation for convenience, then

$$C^{\pm}(\mathbf{x}_A, \mathbf{x}_B) \propto A_{\pm}^2 \sqrt{\frac{2}{\pi kr}} \cos[\omega t \mp (kr - \pi/4)], \tag{4.15}$$

where $C^{\pm}$ refer to the positive ($\theta = 0°$) and negative ($\theta = 180°$) contributions to the integral, respectively. As in the normal-mode case, comparing equation (4.10) with equation (4.15) shows that there is a strong similarity between these expressions and an identity can be made by taking the time derivative of one term, that is

$$\frac{d}{dt} C^{+}(\mathbf{x}_A, \mathbf{x}_B, t) \propto -\omega A_{+}^2 G(\mathbf{x}_A, \mathbf{x}_B, t), \tag{4.16}$$

and a similar identity holds for the second term. Thus, we see that direct evaluation of the cross-correlation and Green's function for surface waves yields a similar identity as in the normal-mode case, as expected. It may also be noted that the identity could have also been written as $C^{+} \propto A_{+}^2 dG/dt$, analogously to equation (4.7).

Unlike the normal-mode framework, this explicit 2D plane-wave framework is also useful in assessing the degree to which a non-uniform noise source distribution causes departures from the expected result. Specifically, one could input arbitrary azimuthal distributions $A(\theta)$ of surface-wave noise sources into equation (4.12) and simply calculate how both the resulting traveltimes and waveforms from noise correlation depart from the expected Green's function traveltimes and waveforms. The integral in equation (4.12) can be evaluated numerically without using the stationary-phase approximation, and requires no assumptions about smoothness as long as sources from different azimuths are uncorrelated. Tests of this nature have previously been done (e.g., Tsai, 2009, 2011; Weaver et al., 2011) and suggest that while traveltimes are typically only affected to second order, due to the stationary phase regions still dominating, amplitudes and hence waveforms can easily be affected to first order.

4.4 Representation Theorems

An alternative justification of Green's function retrieval by interstation correlation can be derived using representation theorems that relate a wavefield to its sources via the Green's function (e.g., Aki and Richards, 2002). In the following paragraphs we will outline the basics of this theory, borrowing essential concepts from the

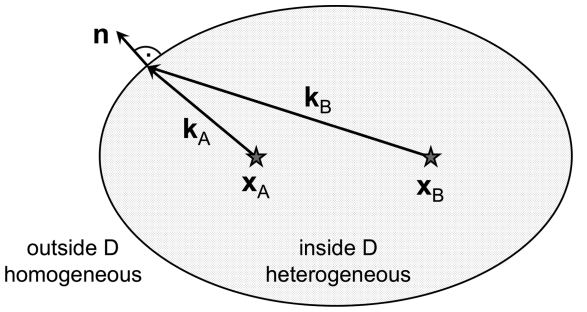

Figure 4.3. Illustration of the two receivers $\mathbf{x}_A$ and $\mathbf{x}_B$ located inside the potentially heterogeneous domain D. The medium at and outside the boundary ∂D is assumed to be homogeneous so that waves only propagate outwards and not inwards. Furthermore, the wavenumber vectors $\mathbf{k}_A$ and $\mathbf{k}_B$ are assumed to be approximately parallel to the boundary normal vector $\mathbf{n}$, which requires a nearly spherical shape of the boundary. To justify the assumption of purely outward-propagating plane waves, the medium also has to be "sufficiently" homogeneous within a region along the inside of the boundary.

work of Wapenaar (2004) and Wapenaar and Fokkema (2006). For educational reasons we will start with the simpler, though for most of the Earth unrealistic, acoustic case, before transitioning to fully elastic wave propagation.

4.4.1 Acoustic Waves

As illustrated in Figure 4.3, we consider a domain D with boundary ∂D within which the two receivers $\mathbf{x}_A$ and $\mathbf{x}_B$ are located. For convenience, we work in the frequency domain, where the acoustic wave equation (4.1) takes the form

$$-\omega^2 \frac{1}{\kappa(\mathbf{x})} u_A(\mathbf{x},\omega) - \frac{\partial}{\partial x_i}\left(\frac{1}{\rho(\mathbf{x})}\frac{\partial}{\partial x_i} u_A(\mathbf{x},\omega)\right) = f_A(\mathbf{x},\omega), \tag{4.17}$$

with the source f_A exciting the wave state u_A. A second source f_B is assumed to excite the wave state u_B that satisfies the wave equation

$$-\omega^2 \frac{1}{\kappa(\mathbf{x})} u_B(\mathbf{x},\omega) - \frac{\partial}{\partial x_i}\left(\frac{1}{\rho(\mathbf{x})}\frac{\partial}{\partial x_i} u_B(\mathbf{x},\omega)\right) = f_B(\mathbf{x},\omega). \tag{4.18}$$

Multiplying the complex conjugate of equation (4.17) with u_B, and equation (4.18) with the complex conjugate of u_A, yields the following pair of equations,

$$-\omega^2 \frac{1}{\kappa(\mathbf{x})} u_A^*(\mathbf{x}) u_B(\mathbf{x}) - u_B(\mathbf{x})\frac{\partial}{\partial x_i}\left(\frac{1}{\rho(\mathbf{x})}\frac{\partial}{\partial x_i} u_A^*(\mathbf{x})\right) = u_B(\mathbf{x}) f_A^*(\mathbf{x}), \tag{4.19}$$

$$-\omega^2 \frac{1}{\kappa(\mathbf{x})} u_A^*(\mathbf{x}) u_B(\mathbf{x}) - u_A^*(\mathbf{x})\frac{\partial}{\partial x_i}\left(\frac{1}{\rho(\mathbf{x})}\frac{\partial}{\partial x_i} u_B(\mathbf{x})\right) = u_A^*(\mathbf{x}) f_B(\mathbf{x}), \tag{4.20}$$

where we omitted dependencies on ω in the interest of a more succinct notation. Equations (4.19) and (4.20) are valid under the assumption that the acoustic medium is not attenuating, meaning that the frequency-domain bulk modulus κ is a real-valued quantity.

Subtracting equation (4.20) from equation (4.19), and integrating over an arbitrary domain D, gives

$$\int_D \left[u_A^*(\mathbf{x}) \frac{\partial}{\partial x_i} \left(\frac{1}{\rho(\mathbf{x})} \frac{\partial}{\partial x_i} u_B(\mathbf{x}) \right) - u_B(\mathbf{x}) \frac{\partial}{\partial x_i} \left(\frac{1}{\rho(\mathbf{x})} \frac{\partial}{\partial x_i} u_A^*(\mathbf{x}) \right) \right] d^3\mathbf{x} = \int_D \left[u_B(\mathbf{x}) f_A^*(\mathbf{x}) - u_A^*(\mathbf{x}) f_B(\mathbf{x}) \right] d^3\mathbf{x}. \tag{4.21}$$

Applying the product rule of differentiation to the left-hand side of equation (4.21) can be written as

$$\begin{aligned} &\int_D \left[\frac{\partial}{\partial x_i} \left(u_A^*(\mathbf{x}) \frac{1}{\rho(\mathbf{x})} \frac{\partial}{\partial x_i} u_B(\mathbf{x}) \right) - \frac{\partial}{\partial x_i} \left(u_B(\mathbf{x}) \frac{1}{\rho(\mathbf{x})} \frac{\partial}{\partial x_i} u_A^*(\mathbf{x}) \right) \right] d^3\mathbf{x} \\ &- \int_D \left[\frac{\partial}{\partial x_i} u_A^*(\mathbf{x}) \frac{1}{\rho(\mathbf{x})} \frac{\partial}{\partial x_i} u_B(\mathbf{x}) - \frac{\partial}{\partial x_i} u_B(\mathbf{x}) \frac{1}{\rho(\mathbf{x})} \frac{\partial}{\partial x_i} u_A^*(\mathbf{x}) \right] d^3\mathbf{x} \\ &= \int_D \left[u_B(\mathbf{x}) f_A^*(\mathbf{x}) - u_A^*(\mathbf{x}) f_B(\mathbf{x}) \right] d^3\mathbf{x}. \end{aligned} \tag{4.22}$$

Realizing that the terms under the second integral in equation (4.22) cancel, we invoke Gauss's theorem to transform the left-hand side into a surface integral,

$$\int_{\partial D} \frac{1}{\rho(\mathbf{x})} \left[u_A^*(\mathbf{x}) \frac{\partial}{\partial x_i} u_B(\mathbf{x}) - u_B(\mathbf{x}) \frac{\partial}{\partial x_i} u_A^*(\mathbf{x}) \right] n_i(\mathbf{x}) \, d^2\mathbf{x} = \int_D \left[u_B(\mathbf{x}) f_A^*(\mathbf{x}) - u_A^*(\mathbf{x}) f_B(\mathbf{x}) \right] d^3\mathbf{x}, \tag{4.23}$$

where n_i is the i-component of the surface normal vector. So far, the sources f_A and f_B are generic, and therefore equation (4.23) represents a general relation between two acoustic wave states in a lossless medium. Specifying the sources as $f_A(\mathbf{x}) = \delta(\mathbf{x}-\mathbf{x}_A)$ and $f_B(\mathbf{x}) = \delta(\mathbf{x}-\mathbf{x}_B)$ determines the solutions; $u_A(\mathbf{x})$ and $u_B(\mathbf{x})$ are the Green's functions $G(\mathbf{x}, \mathbf{x}_A)$ and $G(\mathbf{x}, \mathbf{x}_B)$, respectively. Inserting this into equation (4.23) yields

$$\begin{aligned} 2i \, \mathrm{Im}\, G(\mathbf{x}_A, \mathbf{x}_B) &= G(\mathbf{x}_A, \mathbf{x}_B) - G^*(\mathbf{x}_B, \mathbf{x}_A) \\ &= \int_{\partial D} \frac{1}{\rho(\mathbf{x})} \left[G^*(\mathbf{x}, \mathbf{x}_A) \frac{\partial}{\partial x_i} G(\mathbf{x}, \mathbf{x}_B) - G(\mathbf{x}, \mathbf{x}_B) \frac{\partial}{\partial x_i} G^*(\mathbf{x}, \mathbf{x}_A) \right] n_i(\mathbf{x}) \, d^2\mathbf{x}, \end{aligned} \tag{4.24}$$

where we also invoked reciprocity, $G(\mathbf{x}_A, \mathbf{x}_B) = G(\mathbf{x}_B, \mathbf{x}_A)$ (e.g., Aki and Richards, 2002). Equation (4.24) is not yet particularly useful for interferometry.

It requires further simplifications based on assumptions and approximations that need to be assessed on a case-by-case basis.

The first set of assumptions is that the domain is homogeneous around and outside the boundary ∂D that we require to be nearly spherical in shape and sufficiently far from both $\mathbf{x}_A$ and $\mathbf{x}_B$. This allows us to approximate the Green's function at the boundary ∂D as a plane wave propagating exclusively *out* of the domain and not into the domain, that is

$$G(\mathbf{x}, \mathbf{x}_X) \approx A_X \, e^{-ik\mathbf{n}\cdot\mathbf{x}}, \quad \text{with either } X = A \text{ or } X = B, \tag{4.25}$$

and the amplitude of the wave state is A_X. The wavenumber k satisfies the dispersion relation $k = \omega/c$, with the acoustic velocity $c = \sqrt{\kappa/\rho}$. This setup is illustrated in Figure 4.3. Under the plane-wave assumption, the spatial derivative $\partial/\partial x_i$ results in multiplication by $-ikn_i$ for $G(\mathbf{x}, \mathbf{x}_B)$ and ikn_i for $G^*(\mathbf{x}, \mathbf{x}_A)$. This condenses equation (4.24) to

$$\operatorname{Im} G(\mathbf{x}_A, \mathbf{x}_B) \approx -\frac{\omega}{c'\rho'} \int_{\partial D} G(\mathbf{x}, \mathbf{x}_B) G^*(\mathbf{x}, \mathbf{x}_A) \, d^2\mathbf{x}, \tag{4.26}$$

where ρ' and c' are density and velocity evaluated at the domain boundary ∂D. To relate the Green's functions in equation (4.26) to the propagation of ambient seismic noise, we consider noise sources, $N(\mathbf{x})$, distributed along the boundary ∂D. When averaged, we assume sources at position $\mathbf{x}$ to be temporally uncorrelated with sources at position $\mathbf{y}$, that is

$$S(\mathbf{x}) \, \delta(\mathbf{x} - \mathbf{y}) = \langle N(\mathbf{x}) N^*(\mathbf{y}) \rangle, \tag{4.27}$$

where $\langle \, . \, \rangle$ denotes averaging. The frequency-domain quantity $S(\mathbf{x})$ is the power-spectral density distribution of the noise sources, which we assume to be spatially homogeneous, and denoted simply by S. Multiplying the left-hand sides and the right-hand sides of equations (4.26) and (4.27), and integrating over the boundary ∂D, gives

$$S \operatorname{Im} G(\mathbf{x}_A, \mathbf{x}_B) \approx -\frac{\omega}{c'\rho'} \langle \iint_{\partial D} G(\mathbf{x}, \mathbf{x}_B) N(\mathbf{x}) \, G^*(\mathbf{y}, \mathbf{x}_A) N^*(\mathbf{y}) \, d^2\mathbf{x} \, d^2\mathbf{y} \rangle. \tag{4.28}$$

The surface δ-function has been eliminated by the integration. In equation (4.28) we recognize two representation theorems for a wavefield u excited by the noise sources N and recorded at $\mathbf{x}_A$ and $\mathbf{x}_B$, respectively:

$$u(\mathbf{x}_{A,B}) = \int_{\partial D} G(\mathbf{x}, \mathbf{x}_{A,B}) N(\mathbf{x}) \, d\mathbf{x}. \tag{4.29}$$

Combining equations (4.28) and (4.29), we obtain our final result,

$$G(\mathbf{x}_A, \mathbf{x}_B) - G^*(\mathbf{x}_A, \mathbf{x}_B) \approx -\frac{2i\omega}{Sc'\rho'} C(\mathbf{x}_B, \mathbf{x}_A). \tag{4.30}$$

where $C(\mathbf{x}_B, \mathbf{x}_A) = \langle u(\mathbf{x}_B) u^*(\mathbf{x}_A) \rangle$ is the ensemble averaged correlation function in the frequency domain. Equation (4.30) states that the correlation $C(\mathbf{x}_B, \mathbf{x}_A)$ approximates the Green's function between the receivers, $G(\mathbf{x}_A, \mathbf{x}_B)$ minus its time-reversed version $G^*(\mathbf{x}_A, \mathbf{x}_B)$ up to a scaling factor. The required assumptions are: (1) absence of attenuation, (2) a medium that is homogeneous at and outside the boundary ∂D, as well as within a sufficiently wide region along the inside of the boundary, (3) a sufficiently large distance between the receivers $\mathbf{x}_A$ and $\mathbf{x}_B$ to the domain boundary ∂D, and (4) homogeneously distributed and decorrelated noise sources in the sense of equation (4.27). Items (2) and (3) are needed to justify the approximation of the Green's function in terms of purely outward-propagating plane waves.

4.4.2 Elastic Waves

To derive an analogue of equation (4.30) for elastic waves propagating through the solid Earth's interior, we adapt the concepts used in the previous paragraphs on acoustic waves. As we will see, however, additional complications arise due to the presence of more than one wave type, that is, at least P and S-waves for the simplest case of a homogeneous isotropic medium. These complications will require us to make more severe assumptions and simplifications. The propagation of elastic waves is governed by the elastic wave equation, written in the frequency domain as

$$-\omega^2 \rho(\mathbf{x}) u_i(\mathbf{x}, \omega) - \frac{\partial}{\partial x_j} \left[c_{ijkl}(\mathbf{x}) \frac{\partial}{\partial x_k} u_l(\mathbf{x}, \omega) \right] = f_i(\mathbf{x}, \omega). \tag{4.31}$$

Again omitting dependencies on ω, the i-component of the Green's function due to a force in p-direction, $G_{ip}(\mathbf{x}, \mathbf{x}_A)$, is defined as solution of equation (4.31) when the right-hand side is point-localized in time at $t = 0$ and space at $\mathbf{x} = \mathbf{x}_A$, that is

$$f_i(\mathbf{x}) = \delta_{ip}\, \delta(\mathbf{x} - \mathbf{x}_A) \quad \rightarrow \quad u_i(\mathbf{x}) = G_{ip}(\mathbf{x}, \mathbf{x}_A), \tag{4.32}$$

where δ_{ip} denotes the Kronecker delta. Using equations (4.31) and (4.32), we can follow exactly the same steps as in the acoustic case: (1) Define two states, A and B, (2) multiply the equations for these two states by the other state, respectively, (3) subtract the resulting equations, (4) integrate over the volume D, and (5) apply Gauss's theorem. Again under the assumption that c_{ijkl} is real-valued, meaning that the medium is not attenuating, we find the elastic version of equation (4.24):

$$2i\, \mathrm{Im}\, G_{pq}(\mathbf{x}_A, \mathbf{x}_B) = \int_{\partial D} \left[G^*_{ip}(\mathbf{x}, \mathbf{x}_A) c_{ijkl}(\mathbf{x}) \frac{\partial}{\partial x_k} G_{lq}(\mathbf{x}, \mathbf{x}_B) - G_{iq}(\mathbf{x}, \mathbf{x}_B) c_{ijkl}(\mathbf{x}) \frac{\partial}{\partial x_k} G^*_{lp}(\mathbf{x}, \mathbf{x}_A) \right] n_j(\mathbf{x})\, d^2\mathbf{x}. \tag{4.33}$$

As in the acoustic case, equation (4.33) requires simplifications to eliminate spatial derivatives and space-dependent medium properties inside the integral. Again, assuming that ∂D is far from the stations, and that the medium is homogeneous and isotropic along and outside the boundary, we may approximate the Green's functions $G_{lp}(\mathbf{x}, \mathbf{x}_A)$ by a plane wave propagating exclusively outwards and parallel to the boundary normal $\mathbf{n}$,

$$G_{lp}(\mathbf{x}, \mathbf{x}_A) \approx P_{lp,A} e^{-ik_P \mathbf{n}\cdot\mathbf{x}} + S_{lp,A} e^{-ik_S \mathbf{n}\cdot\mathbf{x}}. \tag{4.34}$$

Since the medium is assumed isotropic, equation (4.34) contains a P-wave with polarization vector $P_{lp,A}$ and wavenumber $k_P = \omega/c_P$, and an S-wave with polarization vector $S_{lp,A}$ and wavenumber $k_S = \omega/c_S$. Taking the spatial derivative $\partial/\partial x_k$ of equation (4.34),

$$\partial_k G_{lp}(\mathbf{x}, \mathbf{x}_A) \approx -in_k \left(P_{lp,A} k_P e^{-ik_P \mathbf{n}\cdot\mathbf{x}} + S_{lp,A} k_S e^{-ik_S \mathbf{n}\cdot\mathbf{x}} \right). \tag{4.35}$$

The appearance of two wave propagation modes generally leads to cross-terms of P- and S-waves when (4.35) is substituted back into equation (4.33). These cross-terms can only be eliminated with additional assumptions and approximations, several of which have been proposed in the literature (e.g., Wapenaar, 2004; Wapenaar and Fokkema, 2006). Here, we will follow probably the simplest line of arguments, based on the relative size of the P- and S-wave contributions in equation (4.35). For a typical crust we have $c_P/c_S \approx \sqrt{3}$ (e.g., Dziewoński and Anderson, 1981; Kennett et al., 1995). Using the expression for P- and S-wave amplitudes in a homogeneous medium (e.g., Aki and Richards, 2002) yields $S_{lp,A} k_S / P_{lp,A} k_P \approx 5.4$, meaning that the P-wave contribution can be ignored relatively safely. Therefore,

$$\partial_k G_{lp}(\mathbf{x}, \mathbf{x}_A) \approx -in_k S_{lp,A} k_S e^{-ik_S \mathbf{n}\cdot\mathbf{x}}. \tag{4.36}$$

With the help of equation (4.36), we can simplify (4.33) to

$$\operatorname{Im} G_{pq}(\mathbf{x}_A, \mathbf{x}_B) \approx -k_S \int_{\partial D} G_{iq}(\mathbf{x}, \mathbf{x}_B) \left[n_k(\mathbf{x}) c_{ijkl}(\mathbf{x}) n_j(\mathbf{x}) \right] G^*_{lp}(\mathbf{x}, \mathbf{x}_A)\, d^2\mathbf{x}. \tag{4.37}$$

Since the medium is assumed isotropic along ∂D, we can expand the term in square brackets in terms of the Lamé parameters λ and μ,

$$n_k c_{ijkl} n_j = n_k(\lambda \delta_{ij}\delta_{kl} + \mu\delta_{ik}\delta_{jl} + \mu\delta_{il}\delta_{jk}) n_j = (\lambda + \mu) n_i n_l + \mu\delta_{il}. \tag{4.38}$$

Noticing that the product of the normal vector n_l with the transversely polarized S-wave Green's function G^*_{lp} vanishes (because the wave is assumed to propagate parallel to the surface normal), equation (4.37) can now be modified to

$$\operatorname{Im} G_{pq}(\mathbf{x}_A, \mathbf{x}_B) \approx -k_S \mu' \int_{\partial D} G_{iq}(\mathbf{x}, \mathbf{x}_B) \delta_{il} G^*_{lp}(\mathbf{x}, \mathbf{x}_A)\, d^2\mathbf{x}, \tag{4.39}$$

with μ' being the constant shear modulus at the boundary ∂D. It remains to introduce vector-valued noise sources $N_l(\mathbf{x})$ that excite the wavefield

$$u_i(\mathbf{y}) = \int_{\partial D} G_{il}(\mathbf{y}, \mathbf{x}) N_l(\mathbf{x})\, d^2\mathbf{x}. \tag{4.40}$$

Assuming that the sources are on average uncorrelated with vanishing cross-terms in the sense of

$$\langle N_i(\mathbf{x}) N_l^*(\mathbf{y}) \rangle = S \delta_{il} \delta(\mathbf{x} - \mathbf{y}), \tag{4.41}$$

equation (4.39) collapses into an equation for the ensemble-averaged interstation correlation $C_{qp}(\mathbf{x}_B, \mathbf{x}_A) = \langle u_q(\mathbf{x}_B) u_p^*(\mathbf{x}_A) \rangle$:

$$G_{pq}(\mathbf{x}_A, \mathbf{x}_B) - G_{pq}^*(\mathbf{x}_A, \mathbf{x}_B) \approx -\frac{2i\omega\mu'}{S c_S} C_{qp}(\mathbf{x}_B, \mathbf{x}_A). \tag{4.42}$$

In analogy to equation (4.30), equation (4.42) also relates the correlation of the wavefield at positions $\mathbf{x}_A$ and $\mathbf{x}_B$ to the interstation Green's function $G_{pq}(\mathbf{x}_A, \mathbf{x}_B)$. To arrive at this result, we had to make new assumptions in addition to those made in the acoustic case already. These include (1) isotropy along and outside the domain boundary ∂D, (2) the absence of off-diagonal elements in the noise source power-spectral density, in the sense of equation (4.41), and (3) the dominance of S-waves, which allowed us to neglect P-wave propagation. The latter assumption may, for instance, be replaced by assumptions on the relative strength of S- and P-wave sources, without changing the final result (Wapenaar and Fokkema, 2006).

A difficulty of the representation theorem approach outlined above is a quantification of the extent to which the various approximations are actually met. This applies, in particular, to the plane wave approximations that require a hardly quantifiable degree of homogeneity around the domain boundary. As a consequence of the approximations and assumptions, the retrieval of the Green's functions on the left-hand side of equation (4.42) is in practice never exact.

Finally, we note that the previous derivations can also be performed in 2D where the waves may be interpreted as analogs of single-mode surface waves propagating on the Earth's surface. This would merely require the use of 2D Green's functions in the derivations.

4.5 Interferometry Without Green's Function Retrieval

While noise interferometry based on Green's function retrieval is one of the great successes of seismological research in the past 15 years, the fact that few of the assumptions needed for its theoretical justification are met in the Earth remains a concern. Failure to meet these assumptions leads to well-documented errors in traveltimes, amplitudes, and waveforms that may become serious problems in

application where high precision is needed, for instance, in time-lapse monitoring of fault zones, volcanoes, and reservoirs.

An alternative to interferometry by Green's function retrieval, with potential to circumvent these issues, was proposed in helioseismology, before interferometry emerged as a major research field in geophysics (Woodard, 1997; Gizon and Birch, 2002). The fundamental idea is to take a correlation function as what it is, not trying to approximate a Green's function. Being a deterministic time series, the correlation function is related via sensitivity kernels to the variations in noise sources and Earth structure that we are eventually interested in. This leads to a coupled inverse problem where both sources and structure need to be constrained, similar to earthquake tomography. Alternatively, information on noise sources from ocean-wave models (e.g., Ardhuin et al., 2011; Gualtieri et al., 2013, 2014; Ardhuin et al., 2015; Gualtieri et al., 2015; Farra et al., 2016) may be incorporated.

Starting again with the acoustic case, we will outline key elements of this theory in the following paragraphs. Subsequently, we briefly summarize the generalization to elastic wave propagation, and provide a range of examples. A more detailed treatment may be found in Tromp et al. (2010), Hanasoge (2013), or Fichtner et al. (2017a).

4.5.1 Modeling Correlation Functions

We start with the acoustic representation theorem (4.29) that expresses the frequency-domain interstation correlation in terms of the sources N and the Green's function $G(\mathbf{m})$ for a suitable Earth model $\mathbf{m}$. Multiplying $u(\mathbf{x}_A)$ with $u^*(\mathbf{x}_B)$ and using the representation theorem yields an expression for the time-domain correlation function,

$$u(\mathbf{x}_A)u^*(\mathbf{x}_B) = \int\int_{\partial D} G(\mathbf{x}, \mathbf{x}_A)G^*(\mathbf{y}, \mathbf{x}_B)N(\mathbf{x})N^*(\mathbf{y})\, d\mathbf{x}\, d\mathbf{y}. \tag{4.43}$$

The domain boundary ∂D is taken to be the surface of the Earth where most noise sources are located. However, the integral can be extended to a volume, if needed. The dependence of G on $\mathbf{m}$ is omitted to avoid clutter. When the noise sources are uncorrelated in the sense of equation (4.27), the ensemble average of equation (4.43) is given by

$$C(\mathbf{x}_A, \mathbf{x}_B) = \langle u(\mathbf{x}_A)u^*(\mathbf{x}_B)\rangle = \int_{\partial D} G(\mathbf{x}, \mathbf{x}_A)G^*(\mathbf{x}, \mathbf{x}_B)S(\mathbf{x})\, d\mathbf{x}. \tag{4.44}$$

Equation (4.44) constitutes a deterministic relation between the correlation $C(\mathbf{x}_A, \mathbf{x}_B)$, the Earth model $\mathbf{m}$, and the noise-source power spectral density $S(\mathbf{x})$, which is allowed to be spatially variable. It implies that $C(\mathbf{x}_A, \mathbf{x}_B)$ can be

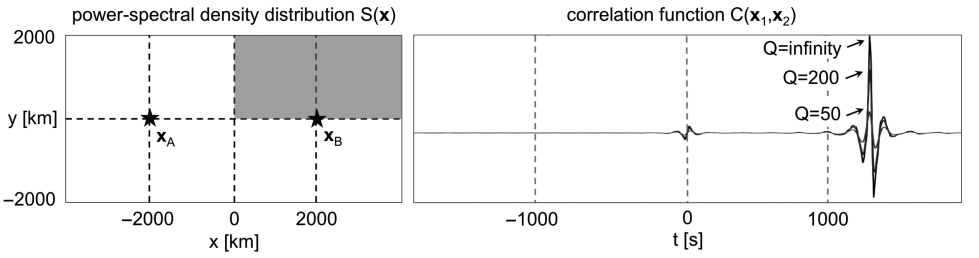

Figure 4.4. Simulation of correlation functions. The source power-spectral density is nonzero only in the gray-shaded region in the left panel. The resulting correlation functions for various Q values are shown to the right for a frequency band from 10 and 30 mHz. (Figure modified from Fichtner (2015).)

modeled without the need to simulate long-duration noise wavefields, and without constraints on the medium properties and the distribution of noise sources.

Figure 4.4 illustrates the simulation of noise correlations in a two-dimensional domain with homogeneous bulk modulus $\kappa = 2.7 \cdot 10^{10}$ N/m^2, density $\rho = 3000$ kg/m^3, and Q taking the values 50, 200, and ∞. Noise sources in the form of nonzero power-spectral density S are located in the gray-shaded region. Due to the heterogeneous source distribution, the correlation function is mostly one-sided with an additional low-amplitude phase around $t = 0$.

To estimate S and $\mathbf{m}$, the simulated correlation $C(\mathbf{x}_A, \mathbf{x}_B)$ must be compared to an observed correlation $C^o(\mathbf{x}_A, \mathbf{x}_B)$. In the interest of simplicity, we assume for the moment that this comparison is done through the computation of the L_2 waveform misfit,

$$\chi = \frac{1}{2} \int [C(\mathbf{x}_A, \mathbf{x}_B, \omega) - C^o(\mathbf{x}_A, \mathbf{x}_B, \omega)]^2 \, d\omega. \tag{4.45}$$

Using Parseval's theorem, equation (4.45) can also be written in the time-domain form

$$\chi = \frac{1}{2} \int [C(\mathbf{x}_A, \mathbf{x}_B, t) - C^o(\mathbf{x}_A, \mathbf{x}_B, t)]^2 \, dt, \tag{4.46}$$

which is, however, less convenient for our purpose. In response to infinitesimal perturbations of the noise sources δS and the Earth model $\delta\mathbf{m}$, the simulated correlation is perturbed from C to $C + \delta C$, which in turn induces a perturbation of the misfit from χ to $\chi + \delta\chi$. Knowing the relation between the perturbations δS and $\delta\mathbf{m}$ would allow us to construct models of noise sources S and Earth structure $\mathbf{m}$ such that the misfit χ is minimized. This relation between model and misfit perturbations can be written in terms of Fréchet or sensitivity kernels that we will derive in the following paragraphs.

4.5.2 Sensitivity Kernels for Noise Sources

Using equation (4.45), the misfit perturbation $\delta\chi = \chi(C+\delta C) - \chi(C)$ is given by

$$\delta\chi = \int [C(\mathbf{x}_A, \mathbf{x}_B) - C^o(\mathbf{x}_A, \mathbf{x}_B)]\, \delta C(\mathbf{x}_A, \mathbf{x}_B)\, d\omega. \tag{4.47}$$

Assuming that perturbations of the correlation function, δC, arise from perturbations in the power-spectral density, δS, we find a relation between $\delta\chi$ and δS with the help of the forward modeling equation (4.44):

$$\delta\chi = \int_{\partial D} \int [C(\mathbf{x}_A, \mathbf{x}_B) - C^o(\mathbf{x}_A, \mathbf{x}_B)]\, G(\mathbf{x}, \mathbf{x}_A) G^*(\mathbf{x}, \mathbf{x}_B) \delta S(\mathbf{x})\, d\omega\, d\mathbf{x}. \tag{4.48}$$

To simplify equation (4.48), we define the noise source kernel K_s as

$$K_s(\mathbf{x}) = \int [C(\mathbf{x}_A, \mathbf{x}_B) - C^o(\mathbf{x}_A, \mathbf{x}_B)]\, G(\mathbf{x}, \mathbf{x}_A) G^*(\mathbf{x}, \mathbf{x}_B)\, d\omega. \tag{4.49}$$

The relation between a perturbation of the noise sources, δS, and the resulting perturbation of the misfit, $\delta\chi$, is now given by

$$\delta\chi = \int_{\partial D} K_s(\mathbf{x})\, \delta S(\mathbf{x})\, d\mathbf{x}. \tag{4.50}$$

The kernel K_s captures the spatial sensitivity of the measurement to the noise sources. In regions where K_s attains large positive values, a positive perturbation of the sources leads to an increase of the misfit, and vice versa. Solving an inverse problem for the noise sources involves finding perturbations δS of an initial noise source model S such that the misfit is minimized.

The waveform misfit introduced in equation (4.45) is only one of many possible ways to quantify the difference between observed and simulated correlation functions. Other misfits may be better suited for specific applications. One example is the travel time misfit used in transmission tomography. Regardless of the specific choice, the misfit variation, $\delta\chi$, can generally be written in the form

$$\delta\chi = \int f\, \delta C(\mathbf{x}_A, \mathbf{x}_B)\, d\omega, \tag{4.51}$$

with a frequency-dependent function f, called the adjoint source (e.g., Fichtner et al., 2017a). In the specific case of the L_2 waveform difference, given in equation (4.47), we have $f = C(\mathbf{x}_A, \mathbf{x}_B) - C^o(\mathbf{x}_A, \mathbf{x}_B)$.

Examples of source kernels for travel time measurements (Luo and Schuster, 1991) on the large-amplitude arrival in Figure 4.4 are shown in Figure 4.5 as a function of attenuation and bandwidth. The kernels have the shape of hyperbolic jets, also known as end-fire lobes. As intuitively expected, the kernel decays more quickly with distance from station $\mathbf{x}_B$ as attenuation increases. More oscillatory

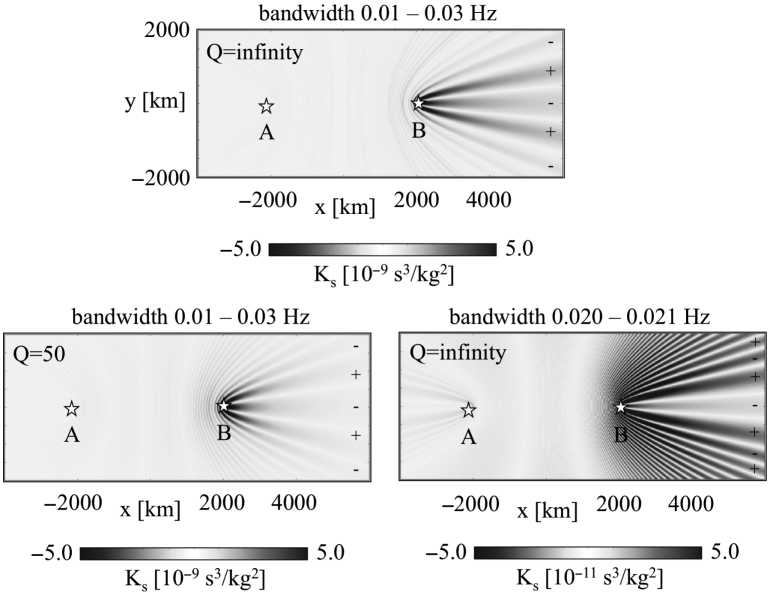

Figure 4.5. Noise source kernels for travel time measurements on the large-amplitude wave in Figure 4.4. The first-order feature is a hyperbolic jet behind station $\mathbf{x}_B$ known as end-fire lobe. Details depend on attenuation, bandwidth and Earth structure. (Figure modified from Fichtner (2015).)

features appear for measurements in a narrower frequency band. It follows that smooth perturbations of S will only contribute when located roughly within the first Fresnel zone along $y = 0$.

4.5.3 Sensitivity Kernels for Earth Structure

The relation between the misfit χ and perturbations in Earth structure, $\delta\mathbf{m}$, are slightly more difficult to derive because $\mathbf{m}$ is not explicit in the forward modeling equation (4.44), but implicit inside the Green's functions. Applying the product rule to equation (4.44), we find the variation of the correlation function in terms of variations of the Green's function,

$$\delta C(\mathbf{x}_A, \mathbf{x}_B) = \int_{\partial D} \left[\delta G(\mathbf{x}, \mathbf{x}_A)\, G^*(\mathbf{x}, \mathbf{x}_B) + G(\mathbf{x}, \mathbf{x}_A)\, \delta G^*(\mathbf{x}, \mathbf{x}_B)\right] S(\mathbf{x})\, d\mathbf{x}. \tag{4.52}$$

With the help of the acoustic wave equation (4.17) we can eliminate δG from equation (4.52). Choosing the force term in the acoustic wave equation (4.1) to be point-localized, that is, $f_A(\mathbf{x}) = \delta(\mathbf{x} - \mathbf{x}_A)$, we obtain the governing equation of the Green's function,

$$-\omega^2 \frac{1}{\kappa(\mathbf{x})} G(\mathbf{x}, \mathbf{x}_A) - \frac{\partial}{\partial x_i}\left(\frac{1}{\rho(\mathbf{x})} \frac{\partial}{\partial x_i} G(\mathbf{x}, \mathbf{x}_A)\right) = \delta(\mathbf{x} - \mathbf{x}_A). \tag{4.53}$$

Perturbing the bulk modulus from κ to $\kappa + \delta\kappa$, and keeping in mind that G depends on κ as well, we obtain the perturbation equation

$$\omega^2 \frac{\delta\kappa(\mathbf{x})}{\kappa^2(\mathbf{x})} G(\mathbf{x}, \mathbf{x}_A) - \omega^2 \frac{1}{\kappa(\mathbf{x})} \delta G(\mathbf{x}, \mathbf{x}_A) = 0. \tag{4.54}$$

Solving equation (4.54) for $\delta G(\mathbf{x}, \mathbf{x}_A)$, and using the corresponding expression for $\delta G(\mathbf{x}, \mathbf{x}_B)$, equation (4.52) transforms to

$$\delta C(\mathbf{x}_A, \mathbf{x}_B) = \int_{\partial D} \frac{\delta\kappa(\mathbf{x})}{\kappa(\mathbf{x})} \left[G(\mathbf{x}, \mathbf{x}_A)\, G^*(\mathbf{x}, \mathbf{x}_B) + G(\mathbf{x}, \mathbf{x}_A)\, G^*(\mathbf{x}, \mathbf{x}_B) \right] S(\mathbf{x})\, d\mathbf{x}. \tag{4.55}$$

Substituting (4.55) into the general expression for the misfit variation (4.51), we finally obtain

$$\delta\chi = \int_{\partial D} K_\kappa(\mathbf{x})\, \delta\kappa(\mathbf{x})\, d\mathbf{x}, \tag{4.56}$$

with the structure kernel

$$K_\kappa(\mathbf{x}) = \int \frac{f\, S(\mathbf{x})}{\kappa(\mathbf{x})} \left[G(\mathbf{x}, \mathbf{x}_A)\, G^*(\mathbf{x}, \mathbf{x}_B) + G(\mathbf{x}, \mathbf{x}_A)\, G^*(\mathbf{x}, \mathbf{x}_B) \right] d\omega. \tag{4.57}$$

The kernel K_κ captures the first-order relation between variations in the bulk modulus κ and the misfit χ. It depends on the noise source power-spectral density S and the adjoint source f, which is determined by the specific choice of a misfit functional. Using the same line of arguments as above, a sensitivity kernel for variations in density, $\delta\rho$, can be derived. Sensitivity kernels for derived medium properties, for instance the acoustic velocity $c = \sqrt{\kappa/\rho}$, follow from the Jacobian rule.

Continuing the examples from the previous figures, Figure 4.6 shows sensitivity kernels for travel time measurements on the large-amplitude arrival at positive times with respect to acoustic velocity. Similar to finite-frequency kernels for surface waves from earthquakes or active sources (e.g., Friederich, 2003; Zhou et al., 2004; Yoshizawa and Kennett, 2005), sensitivity is mostly located between the receiver pair. An additional contribution right of station $\mathbf{x}_B$ results from the heterogeneous distribution of the noise sources.

4.5.4 The Elastic Case

While we have limited ourselves to the acoustic case for pedagogical reasons so far, the previous developments can be translated almost one-to-one to elastic wave propagation that is more relevant for the Earth. Indeed, using the elastic version of the representation theorem (4.40), the cross-correlation matrix can be written in analogy to equation (4.44) as

$$C_{pq}(\mathbf{x}_A, \mathbf{x}_B) = \int_{\partial D} G_{pi}(\mathbf{x}_A, \mathbf{x})\, G^*_{qj}(\mathbf{x}_B, \mathbf{x})\, S_{ij}(\mathbf{x})\, d\mathbf{x}, \tag{4.58}$$

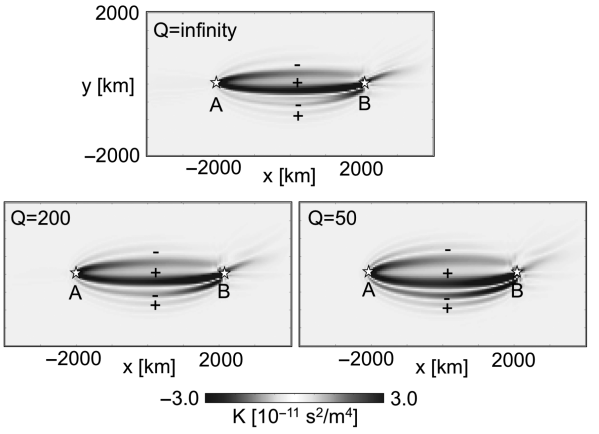

Figure 4.6. Sensitivity kernels for measurements of travel time on the large-amplitude waveform in Figure 4.4 with respect to acoustic velocity c. In contrast to the source kernels, sensitivity is primarily located between the receivers, with an additional contribution right of station $\mathbf{x}_B$ that results from the heterogeneous noise source distribution. The kernels broaden with increasing attenuation, that is, increasing dominance of lower frequencies. (Figure modified from Fichtner (2015).)

where S_{ij} is the power spectral density matrix of the noise sources as a function of space and frequency. Following exactly the same steps taken in sections 4.5.2 and 4.5.3, we can derive sensitivity kernels for noise sources and Earth structure (e.g., Tromp et al., 2010; Fichtner, 2014; Fichtner et al., 2017a),

$$\delta\chi = \int_{\partial D} K_{s,ij}(\mathbf{x})\, S_{ij}(\mathbf{x})\, d\mathbf{x} + \int_D K_i(\mathbf{x}) \delta m_i(\mathbf{x})\, d\mathbf{x}, \tag{4.59}$$

where m_i represents all parameters of an elastic Earth model, for instance P and S velocities, density, and attenuation.

Examples for noise source and Earth structure kernels on the global scale are shown in Figure 4.7. The noise source kernel is computed for the measurement correlation asymmetry of the causal and acausal fundamental-mode surface wave at long periods from 150 to 300 s (Ermert et al., 2016, 2017). Note that the kernel focuses at the antipoles of the two stations. This phenomenon reflects the fact that noise sources at the station antipoles radiate waves that focus at the stations, thereby affecting the correlation amplitudes particularly strongly. The Earth structure kernel is for the measurement of surface wave energy in the causal branch of the correlation function, and with respect to the Lamé parameter λ. Noise sources for this example are homogeneously distributed in the oceans but zero on land.

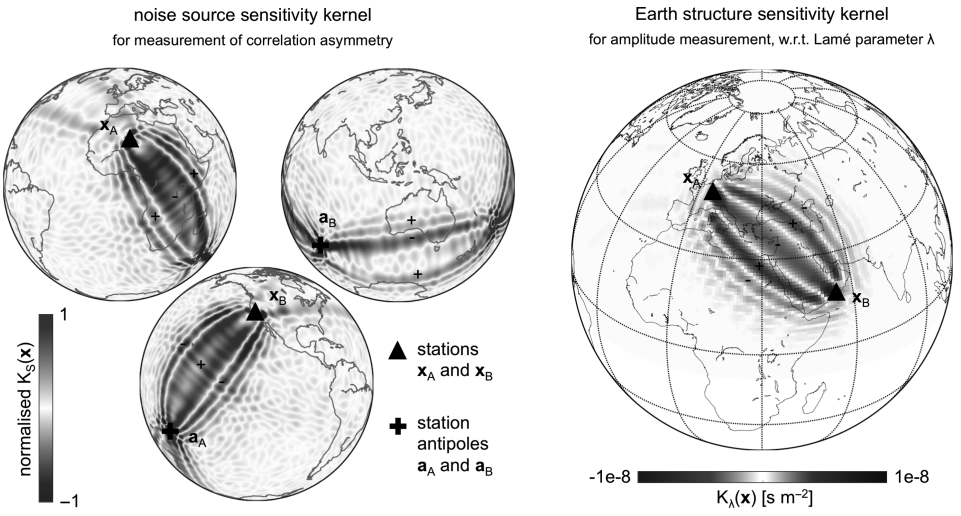

Figure 4.7. Global-scale sensitivity kernels for noise sources and Earth structure. The source distribution used to compute correlation functions is homogeneous and nonzero only in the oceans, and S20RTS (Ritsema et al., 1999) has been used as Earth model. Left: Noise source sensitivity kernel for the measurement of correlation asymmetry between the causal and acausal surface waves at long periods from 150 to 300 s. Note the characteristic focusing of the kernel at the station antipoles. Right: Earth structure sensitivity kernel for the measurement of surface wave energy on the causal branch with respect to the Lamé parameter λ.

These sensitivity kernels provide a quantitative link between measurements on noise correlations and variations in noise sources and Earth structure. With slightly higher algebraic effort, the kernel expressions can be adapted to misfit functionals that may be more suitable than the L_2 waveform misfit of equation (4.45) that we have largely chosen for convenience. Misfit functionals that enable a more differentiated extraction of time- and frequency-dependent differences in phase and amplitude may be found in the recent waveform inversion literature (e.g., Luo and Schuster, 1991; Gee and Jordan, 1992; Fichtner et al., 2008; van Leeuwen and Mulder, 2010; Brossier et al., 2010; Bozdağ et al., 2011; Rickers et al., 2012). The design of suitable measurements that allow us to solve the coupled source/structure inverse problem is an area of active research.

4.6 Discussion

In the following, we provide a summary of the previous mathematical developments in the light of practical applications. Furthermore, we give a brief overview of alternative approaches to interferometry that we do not cover in detail in this chapter due to limited space.

4.6.1 Green's Function Retrieval

The overwhelming majority of noise interferometry studies is based on Green's function retrieval by interstation correlation. The undeniable success of the method is due to its simplicity on multiple levels: The computation of correlation functions is an easy mathematical operation that lends itself very well to implementation on modern supercomputers that allow us to process large quantities of data in reasonable amounts of time (Fichtner et al., 2017b). While the theoretical requirements of Green's function retrieval are generally not met on Earth, at least the frequency-dependent traveltimes (dispersion) of fundamental-mode surface waves are empirically reliable and for most applications sufficiently relatable to the traveltimes of the Green's function. Furthermore, with such an approach, existing techniques for the inversion of earthquake or active-source data can be used to invert noise correlations without the need to develop genuinely new inversion technologies.

The drawback of Green's function retrieval lies in the absence of a theory that applies to the Earth with all its unavoidable complexities, including 3D heterogeneity, attenuation, anisotropy, non-equipartitioned noise, and noise sources that are heterogeneously distributed and highly variable in time. The consequences are, as mentioned in the introduction to this chapter, that traveltimes, amplitudes, and waveforms may be incorrect, and that modern inversion techniques that exploit complete waveforms for improved resolution are therefore not applicable.

In addition to practical limitations of Green's function retrieval, there is a philosophical dilemma. A physical theory is generally valid as long as there are no observations that it cannot explain (e.g., Popper, 1935; Tarantola, 2006). In this regard, the theories for Green's function recovery presented earlier in this chapter are *sensu stricto* invalid because real-data noise correlations typically carry clear signs of not being Green's functions (e.g., spurious arrivals, missing phases). From a pragmatic, though not from a science philosophy, point of view, this problem may be overcome to some extent by ignoring those parts of a noise correlation dataset that are not plausible Green's function approximations.

4.6.2 Interferometry Without Green's Function Retrieval

Interferometry without Green's function retrieval, presented in section 4.5, is designed to function without assumptions on the nature of the ambient noise wavefield and the properties of the Earth and noise sources. A correlation function is modeled on the basis of the noise-source power-spectral density distribution that may vary in time and space. Observable variations in the correlation function can then be related to variations in Earth structure and noise sources, either through model space sampling or via finite-frequency sensitivity kernels.

In addition to being conceptually clean, interferometry without Green's function retrieval offers the opportunity to exploit waveforms in the correlation function that one would not expect in the Green's function. This includes, for instance, early arrivals prior to the P-wave that result from noise sources outside the stationary phase regions.

The most significant drawback of interferometry without Green's function retrieval, which has so far limited its widespread application in geophysics, is increased mathematical and computational complexity. The forward problem cannot be solved simply by computing a Green's function between two receivers, and traditional inversion methods that ignore finite-frequency effects may not be used. Another price to pay for being able to exploit any waveform without restrictive assumptions is the need to account for sources and structure at the same time, which unavoidably increases the model space dimension and the nullspace. As in earthquake tomography, good results can only be achieved when sources and structure are constrained simultaneously (e.g., Valentine and Woodhouse, 2010). This also applies to interferometry based on Green's function retrieval, where a distribution of sources that is incorrectly assumed to be homogeneous may degrade the tomographic images. As an alternative to the joint inversion for source and structure, information from physical noise source models that relate ocean wave height to the noise-source power spectral density may be incorporated in the future (e.g., Ardhuin et al., 2011; Gualtieri et al., 2013, 2014; Ardhuin et al., 2015; Gualtieri et al., 2015; Farra et al., 2016).

While being more involved and still in its infancy, interferometry without Green's function retrieval is producing promising initial results that make future successful applications seem possible (e.g., Hanasoge, 2013; Basini et al., 2013; Delaney et al., 2017; Stehly and Boué, 2017; Ermert et al., 2017; Sager et al., 2018).

4.6.3 The Importance of Processing

In our previous mathematical developments we entirely ignored an essential element of practical ambient noise interferometry: data processing (see Chapter 5 [Ritzwoller and Feng, 2018]). Since the ambient noise wavefield is "polluted" by earthquake signals and excited by sources that are imperfect from the perspective of Green's function recovery, numerous processing and stacking schemes have been proposed in order to obtain more plausible Green's function approximations. These include the averaging of causal and acausal correlation branches, spectral whitening, time-domain running averages, and frequency-domain normalization (e.g., Bensen et al., 2007; Groos et al., 2012), as well as one-bit normalization (e.g., Larose et al., 2004; Shapiro and Campillo, 2004; Cupillard et al., 2011; Hanasoge and Branicki, 2013), phase-weighted stacks based on the Hilbert transform

(Schimmel and Paulssen, 1997; Schimmel et al., 2011) or the S transform (Baig et al., 2009), directional balancing (Curtis and Halliday, 2010), Welch's method of overlapping time windows (Welch, 1967; Seats et al., 2012), the application of curvelet de-noising filters (Stehly et al., 2011), or a sequence of selection and noise suppression filters (e.g., Boué et al., 2014; Nakata et al., 2015).

Despite the large number of noise interferometry studies, a clear consensus on the best processing scheme, however defined, has not emerged. This indicates that the optimal processing is dependent on the specifics of a particular dataset and on the type of information that one wishes to extract. Often, processing is to some extent subjective. Differences in processing can lead to significant differences in the correlation functions (Bensen et al., 2007), which leaves an unavoidable imprint on the sensitivity to Earth structure and noise sources (Fichtner, 2014; Stehly and Boué, 2017). An example of how processing can modify the correlation function is presented in Figure 4.8.

That processing modifies correlation waveforms and their sensitivity is not a problem in itself. However, it may become a problem when not properly taken into account in the forward modeling. From earthquake tomography it is well known that observations and synthetics must be processed in exactly the same way in order to ensure that the sometimes subtle differences between them are indeed

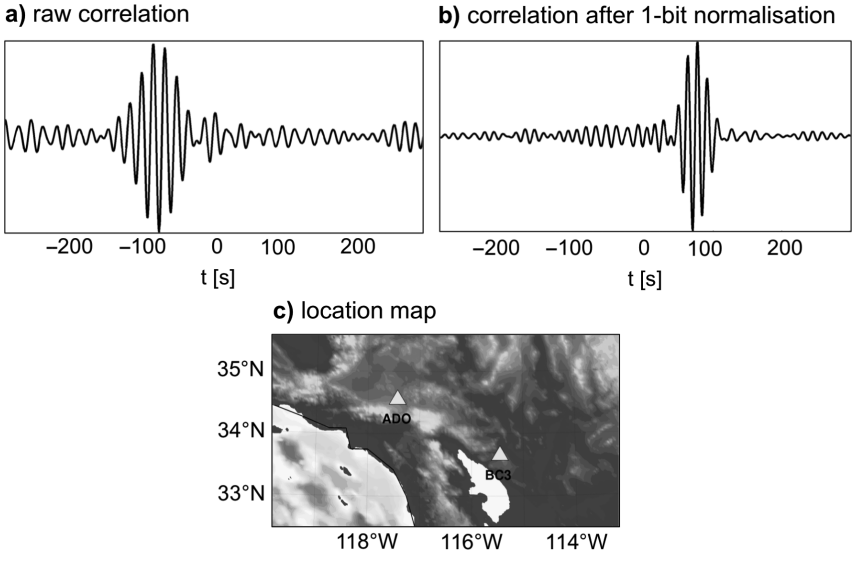

Figure 4.8. Modification of the correlation function between the Californian stations ADO and BC3. (a) Raw correlation function computed without pre-processing of the individual recordings. (b) Correlation function computed after one-bit normalization of the recordings. (c) Location map of stations ADO and BC3. (Figure modified from Fichtner et al. (2017a).)

due to sources or structure. Noise interferometry currently does not operate at the same level of precision, meaning that operations such as various normalizations or elaborate stacking are not taken into account in the forward problem solutions. This may lead to incorrect inferences of structure and sources. While a theory that incorporates noise correlation processing does exist (Fichtner et al., 2017a), it still awaits application to real data.

4.6.4 Alternative Approaches

The early recognition that the theoretical prerequisites of Green's function retrieval are not met on Earth led to the development of a large number of alternative approaches to ambient noise interferometry, only a small fraction of which can be summarized here.

Interferometry by deconvolution (e.g., Snieder and Şafak, 2006; Vasconcelos and Snieder, 2008a,b) replaces the frequency-domain multiplication in correlation by a division. As a result, the interferogram is less dependent on the wavefield source and still an approximation of a Green's function.

Similarly, interferometry by multi-dimensional deconvolution (e.g., Wapenaar et al., 2008; Wapenaar and van der Neut, 2010; Wapenaar et al., 2011) tries to correct for the lack of wavefield equipartitioning. Based on the realization that the virtual source of a noise correlation is not point localized but smeared into a point-spread function, the point-spread function is deconvolved in order to obtain a better Green's function approximation.

Instead of correcting for the imperfections of the noise sources, iterated correlation tries to exploit coda waves (e.g., Stehly et al., 2008). The main rationale is that the coda of a noise correlation may represent a wavefield that is closer to being equipartitioned than the original noise wavefield. Re-correlating the coda should then provide an improved Green's function approximation. The extent to which this approach relies on a homogeneous distribution of scatterers in the Earth remains to be fully explored.

4.7 Conclusions

During the past decade, ambient noise interferometry has profoundly changed the field of seismology. It has substantially increased tomographic resolution in regions without conventional wavefield sources, and it has enabled continuous monitoring of the subsurface.

The large majority of interferometry applications is based on Green's function retrieval by interstation correlation of noise. The success of this approach rests on the easy implementation of the noise correlation operation and on the possibility to reuse inversion methods for earthquake and active-source data almost

without modification. Green's function retrieval can be justified theoretically using a variety of techniques, including normal-mode summation, plane-wave superposition, and representation theorems. The results are generally similar and based on related assumptions of wavefield equipartitioning, the homogeneous distribution of decorrelated noise sources, and the absence of attenuation. Since these assumptions are never satisfied on Earth, noise correlations only approximate Green's functions. The extent to which differences between the two are practically relevant is somewhat application-specific and may be assessed on a case-by-case basis.

Interferometry without Green's function retrieval aims to overcome these limitations by dropping any assumption on equipartitioning, noise source distribution, and wave propagation physics. Noise correlations are taken as what they are, without any attempt to approximate a Green's function. Measurements on noise correlations are related to noise sources and Earth structure via sensitivity kernels that allow us to solve inverse problems. This gain of generality comes at the price of increased computational complexity and the need to solve an inherently coupled inverse problem for both noise sources and Earth structure. First, this will require that source and structure inversion use noise correlations averaged over exactly the same time interval, because noise sources may change over time. Second, it is understood that the independent resolution of noise sources and Earth structure will require adequate coverage, the availability of which is a current topic of research.

The future of ambient noise interferometry is naturally hard to predict. While the basics of interferometry by Green's function retrieval have become standard, continued innovation will likely depend on our ability to exploit more information in a more reliable way. This will involve a combination of both improvements of data processing schemes and improvements of the forward and inverse modeling physics.

Acknowledgments

The authors are grateful to Laura Ermert, Patrick Paitz, Korbinian Sager, Roel Snieder, and an anonymous reviewer for fruitful discussions that helped us to improve this chapter.

References

Aki, K. 1957. Space and time spectra of stationary stochastic waves, with special reference to microtremors. *Bull. Earthq. Res. Inst., Univ. Tokyo*, **35**, 415–457.

Aki, K., and Richards, P. 2002. *Quantitative Seismology.* University Science Books.

Ardhuin, F., Gualtieri, L., and Stutzmann, E. 2018. Physics of ambient noise generation by ocean waves. Pages – of: Nakata, N., Gualtieri, L., and Fichtner, A. (eds.), *Seismic Ambient Noise*. Cambridge University Press, Cambridge, UK.

———. 2015. How ocean waves rock the Earth: Two mechanisms explain microseisms with periods 3 to 300 s. *Geophys. Res. Lett.*, **42**(3), 765–772.

Ardhuin, F., Stutzmann, E., Schimmel, M., and Mangeney, A. 2011. Ocean wave sources of seismic noise. *J. Geophys. Res.*, **116**, doi:10.1029/2011JC006952.

Båth, M. 1968. *Mathematical aspects of seismology*. Elsevier Publishing Company, Amsterdam, London, New York.

Baig, A. M., Campillo, M., and Brenguier, F. 2009. Denoising seismic noise cross correlations. *J. Geophys. Res.*, **114**, doi:10.1029/2008JB006085.

Basini, P., Nissen-Meyer, T., Boschi, L., Casarotti, E., Verbeke, J., Schenk, O., and Giardini, D. 2013. The influence of nonuniform ambient noise on crustal tomography in Europe. *Geochem. Geophys. Geosys.*, **14**, 1471–1492.

Bender, C. M., and Orszag, S. A. 1999. *Advanced Mathematical Methods for Scientists and Engineers: Asymptotic Methods and Perturbation Theory*. Springer, New York.

Bensen, G. D., Ritzwoller, M. H., Barmin, M. P., Levshin, A. L., Lin, F., Moschetti, M. P., Shapiro, N. M., and Yang, Y. 2007. Processing seismic ambient noise data to obtain reliable broad-band surface wave dispersion measurements. *Geophys. J. Int.*, **169**, 1239–1260.

Boschi, L., Weemstra, C., Verbeke, J., Ekström, G., Zunino, A., and Giardini, D. 2013. On measuring surface wave phase velocity from station-station cross-correlation of ambient signal. *Geophys. J. Int.*, **192**, 346–358.

Boué, P., Poli, P., Campillo, M., Pedersen, H., Briand, X., and Roux, P. 2013. Teleseismic correlations of ambient noise for deep global imaging of the Earth. *Geophys. J. Int.*, **194**, 844–848.

Boué, P., Roux, P., Campillo, M., and Briand, X. 2014. Phase velocity tomography of surface waves using ambient noise cross correlation and array processing. *J. Geophys. Res.*, **119**, 519–529.

Bozdağ, E., Trampert, J., and Tromp, J. 2011. Misfit functions for full waveform inversion based on instantaneous phase and envelope measurements. *Geophys. J. Int.*, **185**, 845–870.

Brenguier, F., Campillo, M., Haziioannou, C., Shapiro, N. M., Nadeau, R. M., and Larose, E. 2008a. Postseismic relaxation along the San Andreas fault at Parkfield from continuous seismological observations. *Science*, **321**, 1478–1481.

Brenguier, F., Shapiro, N. M., Campillo, M., Ferrazzini, V., Duputel, Z., Coutant, O., and Nercessian, A. 2008b. Towards forecasting volcanic eruptions using seismic noise. *Nat. Geosci.*, **1**, 126–130.

Brossier, R., Operto, S., and Virieux, J. 2010. Which data residual norm for robust elastic frequency-domain full waveform inversion? *Geophysics*, **75**, R37–R46.

Bussat, S., and Kugler, S. 2011. Offshore ambient-noise surface-wave tomography above 0.1 Hz and its applications. *The Leading Edge*, **May 2011**, 514–524.

Claerbout, J. F. 1968. Synthesis of a layered medium from its acoustic transmission response. *Geophysics*, **33**, 264–269.

Cole, S. P. 1995. *Passive seismic and drill-bit experiments using 2-D arrays*. Ph.D. thesis, The Stanford Exploration Project, Stanford University.

Cupillard, P. 2008. *Simulation par la méthode des éléments spectraux des formes donde obtenues par corrélation de bruit sismique*. PhD thesis, Institut de Physique du Globe de Paris.

Cupillard, P., and Capdeville, Y. 2010. On the amplitude of surface waves obtained by noise correlation and the capability to recover the attenuation: a numerical approach. *Geophys. J. Int.*, **181**, 1687–1700.

Cupillard, P., Stehly, L., and Romanowicz, B. 2011. The one-bit noise correlation: a theory based on the concepts of coherent and incoherent noise. *Geophys. J. Int.*, **184**, 1397–1414.

Curtis, A., and Halliday, D. 2010. Directional balancing for seismic and general wavefield interferometry. *Geophysics*, **75**, doi: 10.1190/1.3298736.

Curtis, A., Gerstoft, P., Sato, H., Snieder, R., and Wapenaar, K. 2006. Seismic interferometry - Turning noise into signal. *The Leading Edge*, **25**, 1082–1092.

de Ridder, S. A. L., and Biondi, B. L. 2015. Ambient seismic noise tomography at Ekofisk. *Geophysics*, **80**, B167–B176.

de Ridder, S. A. L., Biondi, B. L., and Clapp, R. G. 2014. Time-lapse seismic noise correlation tomography at Valhall. *Geophys. Res. Lett.*, **41**, 6116–6122.

Delaney, E., Ermert, L., Sager, K., Kritski, A., Bussat, S., and Fichtner, A. 2017. Passive seismic monitoring with non-stationary noise sources. *Geophysics*, **82**, 10.1190/geo2016–0330.1.

Dziewoński, A. M., and Anderson, D. L. 1981. Preliminary reference Earth model. *Phys. Earth Planet. Inter.*, **25**, 297–356.

Ermert, L., Sager, K., Afanasiev, M., Boehm, C., and Fichtner, A. 2017. Ambient noise source inversion in a heterogeneous Earth - Theory and application to the Earth's hum. *J. Geophys. Res.*, **122**, doi:10.1002/2017JB014738.

Ermert, L., Villasenor, A., and Fichtner, A. 2016. Cross-correlation imaging of ambient noise sources. *Geophys. J. Int.*, **204**, 347–364.

Farra, V., Stutzmann, E., Gualtieri, L., and Ardhuin, F. 2016. Ray-theoretical modeling of secondary microseism P waves. *Geophys. J. Int.*, **206**, 1730–1739.

Fichtner, A. 2014. Source and processing effects on noise correlations. *Geophys. J. Int.*, **197**, 1527–1531.

———. 2015. Source-structure trade-offs in ambient noise correlations. *Geophys. J. Int.*, **202**, 678–694.

Fichtner, A., Kennett, B. L. N., Igel, H., and Bunge, H.-P. 2008. Theoretical background for continental- and global-scale full-waveform inversion in the time-frequency domain. *Geophys. J. Int.*, **175**, 665–685.

———. 2009. Full seismic waveform tomography for upper-mantle structure in the Australasian region using adjoint methods. *Geophys. J. Int.*, **179**, 1703–1725.

Fichtner, A., Ermert, L., and Gokhberg, A. 2017b. Seismic noise correlation on heterogeneous supercomputers. *Seis. Res. Lett.*, 88, 1141–1145.

Fichtner, A., Stehly, L., Ermert, L., and Boehm, C. 2017a. Generalised interferometry - I. Theory for inter-station correlations. *Geophys. J. Int.*, **208**, 603–638.

Forghani, F., and Snieder, R. 2010. Underestimation of body waves and feasibility of surface wave reconstruction by seismic interferometry. *The Leading Edge*, **July 2010**, 790–794.

Friederich, W. 2003. The S-velocity structure of the East Asian mantle from inversion of shear and surface waveforms. *Geophys. J. Int.*, **153**, 88–102.

Froment, B., Campillo, M., Roux, P., Gouédard, P., Verdel, A., and Weaver, R. L. 2010. Estimation of the effect of nonisotropically distributed energy on the apparent arrival time in correlations. *Geophysics*, **75**, SA85–SA93.

Gal, M., and Reading, A. M. 2018. Beamforming and polarization analysis. Pages – of: Nakata, N., Gualtieri, L., and Fichtner, A. (eds.), *Seismic Ambient Noise*. Cambridge University Press, Cambridge, UK.

Gee, L. S., and Jordan, T. H. 1992. Generalized seismological data functionals. *Geophys. J. Int.*, **111**, 363–390.

Gilbert, F. 1970. Excitation of the normal modes of the Earth by earthquake sources. *Geophys. J. R. astr. Soc.*, **22**, 223–226.

Gizon, L., and Birch, A. C. 2002. Time-distance helioseismology: the forward problem for random distributed sources. *Astrophys. J.*, **571**, 966–986.

Groos, J. C., Bussat, S., and Ritter, J. R. R. 2012. Performance of different processing schemes in seismic noise cross-correlations. *Geophys. J. Int.*, **188**, 498–512.

Gualtieri, L., Stutzmann, E., Capdeville, Y., Ardhuin, F., Schimmel, A. M., and Morelli, A. 2013. Modeling secondary microseismic noise by normal mode summation. *Geophys. J. Int.*, **193**, 1732–1745.

Gualtieri, L., Stutzmann, E., Capdeville, Y., Farra, V., Mangeney, A., and Morelli, A. 2015. On the shaping factors of the secondary microseismic wavefield. *J. Geophys. Res.*, **120**, 6241–6262.

Gualtieri, L., Stutzmann, E., Farra, V., Capdeville, Y., Schimmel, M., Ardhuin, F., and Morelli, A. 2014. Modeling the ocean site effect on seismic noise body waves. *Geophys. J. Int.*, **197**, 1096–1106.

Haberman, R. 2013. *Applied Partial Differential Equations*. Pearson.

Halliday, D., and Curtis, A. 2008. Seismic interferometry, surface waves and source distribution. *Geophys. J. Int.*, **175**, 1067–1087.

Hanasoge, S. M. 2013. Measurements and kernels for source-structure inversions in noise tomography. *Geophys. J. Int.*, **192**, 971–985.

Hanasoge, S. M., and Branicki, M. 2013. Interpreting cross-correlations of one-bit filtered noise. *Geophys. J. Int.*, **195**, 1811–1830.

Hanasoge, S. M., Birch, A., Gizon, L., and Tromp, J. 2011. The adjoint method applied to time-distance helioseismology. *Astrophys. J.*, **738**, doi:10.1088/0004–637X/738/1/100.

Haned, A., Stutzmann, E., Schimmel, M., Kiselev, S., Davaille, A., and Yelles-Chaouche, A. 2016. Global tomography using seismic hum. *Geophys. J. Int.*, **204**, 1222–1236.

Hillers, G., Husen, S., Obermann, A., Planes, T., Larose, E., and Campillo, M. 2015. Noise-based monitoring and imaging of aseismic transient deformation induced by the 2006 Basel reservoir stimulation. *Geophysics*, **80**, KS51–KS68.

Huang, H.-H., Lin, F.-C., Tsai, V. C., and Koper, K. D. 2016. High-resolution probing of inner core structure with seismic interferometry. *Geophys. Res. Lett.*, in press.

Igel, H., Djikpesse, H., and Tarantola, A. 1996. Waveform inversion of marine reflection seismograms for P impedance and Poisson's ratio. *Geophys. J. Int.*, **124**, 363–371.

Kao, H., Behr, Y., Currie, C. A., Hyndman, R., Townend, J., Lin, F.-C., Ritzwoller, M. H., Shan, S.-J., and He, J. 2013. Ambient seismic noise tomography of Canada and adjacent regions: Part I. Crustal structures. *J. Geophys. Res.*, **118**, 5865–5887.

Kästle, E. D., Soomro, R., Weemstra, C., Boschi, L., and Meier, T. 2016. Two-receiver measurements of phase velocity of ambient-noise and earthquake-based observations. *Geophys. J. Int.*, **207**, 1493–1512.

Kennett, B. L. N., Engdahl, E. R., and Buland, R. 1995. Constraints on seismic velocities in the Earth from traveltimes. *Geophys. J. Int.*, **122**, 108–124.

Kimman, W., and Trampert, J. 2010. Approximations in seismic interferometry and their effects on surface waves. *Geophys. J. Int.*, **182**, 461–476.

Larose, E., Derode, A., Campillo, M., and Fink, M. 2004. Imaging from one-bit correlations of wideband diffuse wave fields. *J. Appl. Phys.*, **95**, 8393–8399.

Lin, F.-C., Moschetti, M. P., and Ritzwoller, M. H. 2008. Surface wave tomography of the western United States from ambient noise: Rayleigh and Love wave phase velocity maps. *Geophys. J. Int.*, **173**, 281–298.

Lin, F.-C., Tsai, V. C., Schmandt, B., Duputel, Z., and Zhan, Z. 2013. Extracting seismic core phases with array interferometry. *Geophys. Res. Lett.*, **40**, 1049–1053.

Lobkis, O. I., and Weaver, R. L. 2001. On the emergence of the Green's function in the correlations of a diffuse field. *J. Acoust. Soc. Am.*, **110**, 3011–3017.

Luo, Y., and Schuster, G. T. 1991. Wave-equation traveltime inversion. *Geophysics*, **56**, 645–653.

Malcolm, A. E., Scales, J., and van Tiggelen, B. A. 2004. Extracting the Green function from diffuse, equipartitioned waves. *Phys. Rev. E*, **70**, doi:10.1103/PhysRevE.70.015601.

McNamara, D., Boaz, R., and Buland, R. 2018. Visualization of the Ambient Seismic Noise Spectrum. Pages – of: Nakata, N., Gualtieri, L., and Fichtner, A. (eds.), *Seismic Ambient Noise*. Cambridge University Press, Cambridge, UK.

Mordret, A., Landès, M., Shapiro, N., Singh, S., and Roux, P. 2014. Ambient noise surface wave tomography to determine the shallow shear velocity structure at Valhall: depth inversion with a Neighbourhood Algorithm. *Geophysical Journal International*, **198**(3), 1514–1525.

Mordret, A., Landès, M., Shapiro, N., Singh, S., Roux, P., and Barkved, O. 2013. Near-surface study at the Valhall oil field from ambient noise surface wave tomography. *Geophysical Journal International*, ggt061.

Morse, P. M., and Feshbach, H. 1953. *Methods of Theoretical Physics*. McGraw-Hill, New York.

Nakata, N., Chang, J. P., Lawrence, J. F., and Boué, P. 2015. Body wave extraction and tomography at Long Beach, California, with ambient-noise interferometry. *J. Geophys. Res.*, **120**, 1159–1173.

Nishida, K., and Montagner, J.-P. 2009. Global surface wave tomography using seismic hum. *Science*, **326**, 5949.

Nooghabi, A. H., Boschi, L., Roux, P., and de Rosny, J. 2017. Coda reconstruction from cross-correlation of a diffuse field on thin elastic plates. *Phys. Rev. E*, under review.

Obermann, A., Froment, B., Campillo, M., Larose, E., Planes, T., Valette, B., Chen, J.-H., and Liu, Q. Y. 2014. Seismic noise correlations to image structural and mechanical changes associated with the Mw 7.9 2008 Wenchuan earthquake. *J. Geophys. Res.*, **119**, doi:10.1002/2013JB010932.

Obermann, A., Kraft, T., Larose, E., and Wiemer, S. 2015. Potential of ambient seismic noise techniques to monitor the St. Gallen geothermal site (Switzerland). *J. Geophys. Res.*, **120**, doi:10.1002/2014JB011817.

Obermann, A., Planes, T., Larose, E., and Campillo, M. 2013. Imaging preeruptive and coeruptive structural and mechanical changes of a volcano with ambient seismic noise. *J. Geophys. Res.*, **118**, 1–10.

Poli, P., Campillo, M., Pedersen, H., and LAPNET Working Group. 2012. Body-wave imaging of Earth's mantle discontinuities from ambient seismic noise. *Science*, **38**, 1063–1065.

Poli, P., Thomas, C., Campillo, M., and Pedersen, H. 2015. Imaging the D" reflector with noise correlations. *Geophys. Res. Lett.*, **42**, 60–65.

Popper, K. 1935. *Logik der Forschung (The logic of scientific discovery)*. Verlag von Julius Springer, Vienna, Austria.

Pratt, R. G. 1999. Seismic waveform inversion in the frequency domain, Part 1: Theory and verification in a physical scale model. *Geophysics*, **64**, 888–901.

Rickers, F., Fichtner, A., and Trampert, J. 2012. Imaging mantle plumes with instantaneous phase measurements of diffracted waves. *Geophys. J. Int.*, **190**, 650–664.

Ritsema, J., vanHeijst, H., and Woodhouse, J. H. 1999. Complex shear wave velocity structure imaged beneath Africa and Iceland. *Science*, **286**, 1925–1928.

Ritzwoller, M. H., and Feng, L. 2018. Overview of pre- and post-processing of ambient noise correlations. Pages – of: Nakata, N., Gualtieri, L., and Fichtner, A. (eds.), *Seismic Ambient Noise*. Cambridge University Press, Cambridge, UK.

Sabra, K. G., Gerstoft, P., Roux, P., and Kuperman, W. A. 2005. Surface wave tomography from microseisms in Southern California. *Geophys. Res. Lett.*, **32**, doi:10.1029/2005GL023155.

Sager, K., Ermert, L., Boehm, C., and Fichtner, A. 2018. Towards full waveform ambient noise inversion. *Geophys. J. Int.*, **212**, 566–590.

Saygin, E., and Kennett, B. L. N. 2012. Crustal structure of Australia from ambient seismic noise tomography. *J. Geophys. Res.*, **117**, doi:10.1029/2011JB008403.

Schimmel, M., and Paulssen, H. 1997. Noise reduction and detection of weak, coherent signals through phase-weighted stacks. *Geophys. J. Int.*, **130**, 497–505.

Schimmel, M., Stutzmann, E., and Gallart, J. 2011. Using instantaneous phase coherence for signal extraction from ambient noise data at a local to a global scale. *Geophys. J. Int.*, **184**, 494–506.

Seats, K. J., Lawrence, J. F., and Prieto, G. A. 2012. Improved ambient noise correlation functions using Welch's method. *Geophys. J. Int.*, **188**, 513–523.

Sens-Schönfelder, C., and Brenguier, F. 2018. Noise-based monitoring. Pages – of: Nakata, N., Gualtieri, L., and Fichtner, A. (eds.), *Seismic Ambient Noise*. Cambridge University Press, Cambridge, UK.

Shapiro, N. 2018. Applications with surface waves extracted from ambient seismic noise. Pages — of: Nakata, N., Gualtieri, L., and Fichtner, A. (eds.), *Seismic Ambient Noise*. Cambridge University Press, Cambridge, UK.

Shapiro, N. M., and Campillo, M. 2004. Emergence of broadband Rayleigh waves from correlations of the ambient seismic noise. *Geophys. Res. Lett.*, **31**, doi:10.1029/2004GL019491.

Shapiro, N. M., Campillo, M., Stehly, L., and Ritzwoller, M. 2005. High resolution surface wave tomography from ambient seismic noise. *Science*, **307**, 1615–1618.

Snieder, R. 2004a. Extracting the Green's function from the correlation of coda waves: A derivation based on stationary phase. *Phys. Rev. E*, **69**, doi:10.1103/PhysRevE.69.046610.

Snieder, R. 2004b. *Mathematical Methods for the Physical Sciences*. Cambridge University Press, Cambridge.

Snieder, R., and Şafak, E. 2006. Extracting the building response using seismic interferometry: Theory and application to the Millikan Library in Pasadena, California. *Bull. Seis. Soc. Am.*, **96**, 586–598.

Snieder, R., Duran, A., and Obermann, A. 2018. Locating velocity changes in elastic media with coda wave interferometry. Pages – of: Nakata, N., Gualtieri, L., and Fichtner, A. (eds.), *Seismic Ambient Noise*. Cambridge University Press, Cambridge, UK.

Stehly, L., and Boué, P. 2017. On the interpretation of the amplitude decay of noise correlations computed along a line of receivers. *Geophys. J. Int.*, **209**, 358–372.

Stehly, L., Campillo, M., Froment, B., and Weaver, R. L. 2008. Reconstructing Greens function by correlation of the coda of the correlation (C3) of ambient seismic noise. *J. Geophys. Res.*, **113**, doi:10.1029/2008JB005693.

Stehly, L., Cupillard, P., and Romanowicz, B. 2011. Towards improving ambient noise tomography using simultaneously curvelet denoising filters and SEM simulations of seismic ambient noise. *Com. Rend. Geosc.*, **343**, 591–599.

Stehly, L., Fry, B., Campillo, M., Shapiro, N. M., Guilbert, J., Boschi, L., and Giardini, D. 2009. Tomography of the Alpine region from observations of seismic ambient noise. *Geophys. J. Int.*, **178**, 338–350.

Tape, C., Liu, Q., Maggi, A., and Tromp, J. 2010. Seismic tomography of the southern California crust based upon spectral-element and adjoint methods. *Geophys. J. Int.*, **180**, 433–462.

Tarantola, A. 2006. Popper, Bayes and the inverse problem. *Nature Physics*, **2**, 492–494.

Tromp, J., Luo, Y., Hanasoge, S., and Peter, D. 2010. Noise cross-correlation sensitivity kernels. *Geophys. J. Int.*, **183**, 791–819.

Tsai, V. C. 2009. On establishing the accuracy of noise tomography traveltime measurements in a realistic medium. *Geophys. J. Int.*, **178**, 1555–1564.

———. 2010. The Relationship Between Noise Correlation and the Green's Function in the Presence of Degeneracy and the Absence of Equipartition. *Geophys. J. Int.*, **182**, 1509–1514.

———. 2011. Understanding the amplitudes of noise correlation measurements. *J. Geophys. Res.*, **116**, doi:10.1029/2011JB008483.

Valentine, A. P., and Woodhouse, J. H. 2010. Reducing errors in seismic tomography: Combined inversion for sources and structure. *Geophys. J. Int.*, **180**, 847–857.

van Leeuwen, T., and Mulder, W. A. 2010. A correlation-based misfit criterion for wave-equation traveltime tomography. *Geophys. J. Int.*, **182**, 1383–1394.

van Wijk, K. 2006. On estimating the impulse response between receivers in a controlled ultrasonic experiment. *Geophysics*, **71**, SI79–SI84.

Vasconcelos, I., and Snieder, R. 2008a. Interferometry by deconvolution, Part 1 – Theory for acoustic waves and numerical examples. *Geophysics*, **73**, S129–S141.

Vasconcelos, I., and Snieder, R. 2008b. Interferometry by deconvolution, Part 2 – Theory for elastic waves and application to drill-bit seismic imaging. *Geophysics*, **73**, S115–S128.

Verbeke, J., Boschi, L., Stehly, L., Kissling, E., and Michelini, A. 2012. High-resolution Rayleigh-wave velocity maps of central Europe from a dense ambient-noise data set. *Geophys. J. Int.*, **188**, 1173–1187.

Wapenaar, K. 2004. Retrieving the elastodynamic Green's function of an arbitrary inhomogeneous medium by cross correlation. *Phys. Rev. Lett.*, **93**, 254301.

Wapenaar, K., and Fokkema, J. 2006. Green's function representations for seismic interferometry. *Geophysics*, **71**, SI33–SI46.

Wapenaar, K., and van der Neut, J. 2010. A representation for Greens function retrieval by multidimensional deconvolution. *J. Acoust. Soc. Am.*, **128**, 366–371.

Wapenaar, K., Ruigrok, E., van der Neut, J., and Draganov, D. 2011. Improved surface-wave retrieval from ambient seismic noise by multi-dimensional deconvolution. *Geophys. Res. Lett.*, **38**, doi:10.1029/2010GL045523.

Wapenaar, K., van der Neut, J., and Ruigrok, E. 2008. Passive seismic interferometry by multidimensional deconvolution. *Geophysics*, **73**, A51–A56.

Watson, G. N. 2008. *A Treatise on the Theory of Bessel Functions*. Merchant Books, LaVergne.

Weaver, R. L., and Lobkis, O. I. 2004. Diffuse fields in open systems and the emergence of Green's function. *J. Acoust. Soc. Am.*, **116**, 2731–2734.

Weaver, R. L., Hadziioannou, C., Larose, E., and Campillo, M. 2011. On the precision of noise correlation interferometry. *Geophys. J. Int.*, **185**, 1384–1392.

Welch, P. D. 1967. The use of fast Fourier transform for the estimation of power spectra: A method based on time-averaging over short, modified periodograms. *IEEE Trans. Audio Electroacoust.*, **15**, 70–73.

Woodard, M. F. 1997. Implications of localized, acoustic absorption for heliotomographic analysis of sunspots. *Astrophys. J.*, **485**, 890–894.

Yoshizawa, K., and Kennett, B. L. N. 2004. Multi-mode surface wave tomography for the Australian region using a 3-stage approach incorporating finite-frequency effects. *J. Geophys. Res.*, **109**, doi:10.1029/2002JB002254.

———. 2005. Sensitivity kernels for finite-frequency surface waves. *Geophys. J. Int.*, **162**, 910–926.

Zhou, Y., Dahlen, F. A., and Nolet, G. 2004. Three-dimensional sensitivity kernels for surface wave observables. *Geophys. J. Int.*, **158**, 142–168.

Zhou, Y., Nolet, G., Dahlen, F. A., and Laske, G. 2006. Global upper-mantle structure from finite-frequency surface-wave tomography. *J. Geophys. Res.*, **111**, doi:10.1029/2005JB003677.

Zheng, Y., Shen, W., Zhou, L., Yang, Y., Xie, Z., and Ritzwoller, M. 2011. Crust and uppermost mantle beneath the North China Craton, northeastern China, and the Sea of Japan from ambient noise tomography. *J. Geophys. Res.*, **116**.